

University of Montana

ScholarWorks at University of Montana

Graduate Student Theses, Dissertations, &
Professional Papers

Graduate School

2004

Ground penetrating radar and seismic refraction as tools to characterize shallow subsurface conditions on Tongass National Forest Alaska

Noel S. Philip
The University of Montana

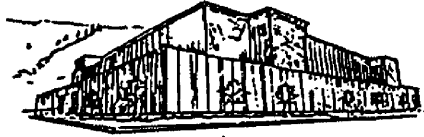
Follow this and additional works at: <https://scholarworks.umt.edu/etd>

Let us know how access to this document benefits you.

Recommended Citation

Philip, Noel S., "Ground penetrating radar and seismic refraction as tools to characterize shallow subsurface conditions on Tongass National Forest Alaska" (2004). *Graduate Student Theses, Dissertations, & Professional Papers*. 8156.
<https://scholarworks.umt.edu/etd/8156>

This Thesis is brought to you for free and open access by the Graduate School at ScholarWorks at University of Montana. It has been accepted for inclusion in Graduate Student Theses, Dissertations, & Professional Papers by an authorized administrator of ScholarWorks at University of Montana. For more information, please contact scholarworks@mso.umt.edu.



**Maureen and Mike
MANSFIELD LIBRARY**

The University of
Montana

Permission is granted by the author to reproduce this material in its entirety, provided that this material is used for scholarly purposes and is properly cited in published works and reports.

****Please check "Yes" or "No" and provide signature****

Yes, I grant permission

No, I do not grant permission

Author's Signature: _____

Date: _____

Maureen and Mike Mansfield
04/20/04

Any copying for commercial purposes or financial gain may be undertaken only with the author's explicit consent.

Ground Penetrating Radar and Seismic Refraction as Tools to
Characterize Shallow Subsurface Conditions on Tongass
National
Forest, Alaska

By

Noel S. Philip

B.Sc., The University of Montana, 2002

Presented in partial fulfillment of the requirements
For the degree of Master of Science

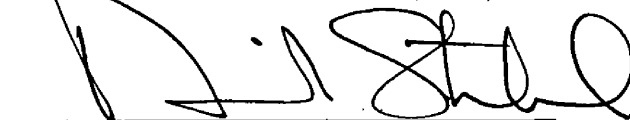
The University of Montana

2004

Approved by:



Chairman



Dean, Graduate School

5-25-04

Date

UMI Number: EP38957

All rights reserved

INFORMATION TO ALL USERS

The quality of this reproduction is dependent upon the quality of the copy submitted.

In the unlikely event that the author did not send a complete manuscript and there are missing pages, these will be noted. Also, if material had to be removed, a note will indicate the deletion.



UMI EP38957

Published by ProQuest LLC (2013). Copyright in the Dissertation held by the Author.

Microform Edition © ProQuest LLC.

All rights reserved. This work is protected against unauthorized copying under Title 17, United States Code



ProQuest LLC.
789 East Eisenhower Parkway
P.O. Box 1346
Ann Arbor, MI 48106 - 1346

Ground Penetrating Radar and Seismic Refraction as tools to Characterize Shallow Subsurface Conditions on Tongass National Forest, Alaska

Department Chair: Steven D. Sheriff



Ground penetrating radar (GPR) and seismic refraction surveys conducted at a critical location on a glacial moraine near Yakutat, Alaska reveal its inferred stratigraphy. The moraine material observed from exposures and shallow excavation is composed of material ranging in size from medium sand to boulders >1m in diameter. Seismic data acquired on the moraine show a subsurface depth to refractor of ~10-15 meters. GPR images show events that reveal the stratigraphy to bedrock depth at 30m. The stratigraphy is like that seen at outcrops 10km northeast. With this interpretation, I produced a reasonable subsurface stratigraphy that identifies hydrogeologic units and depth to bedrock with one meter estimated resolution of depth (10%). The subsurface model provides valuable insight to potential stream incision during the next cyclical closure of Russell Fjord by Hubbard Glacier, the water body bordering the glacial moraine to the north. Based on the sediment depth, there does not appear to be any danger of them being scoured to bedrock.

GPR and seismic refraction surveys conducted at a different site, a Forest Service road near Petersburg, Alaska, help measure depth to bedrock and the water table. Data collected at several culvert sites show classic hyperbolic response from the GPR in imaging cultural artifacts. Engineering plans, made during construction, provide known depths to reflectors allowing radar wave velocity to be derived at each location, promoting the calculation of accurate depth to reflectors.

TABLE OF CONTENTS - TEXT

ABSTRACT ii, 1

TABLE OF CONTENTS iii

LIST OF FIGURES iv

**PART I. HYDROGEOLOGIC UNIT CHARACTERIZATION ON A RECENTLY ACTIVE
GLACIAL MORaine USING GROUND PENETRATING RADAR AND SEISMIC
REFRACTION**

INTRODUCTION 1

METHODS 7

RESULTS 15

**IMAGE INTERPRETATION AND DISCUSSION OF DERIVED SUBSURFACE PROPERTIES
20**

**PART II. LOCATING BEDROCK SURFACES IN AREAS WITH KNOWN FEATURES
USING GROUND PENETRATING RADAR AND SEISMIC REFRACTION**

INTRODUCTION 28

METHODS 30

RESULTS AND DISCUSSION 31

BENEFITS AND LIMITATIONS OF GPR AT CULVERT SITES 35

TABLE OF CONTENTS – COMPACT DISK

FILENAME: APPENDIX.PDF (ADOBE® PORTABLE DOCUMENT FORMAT)

APPENDIX A-1: SPILLWAY GPR IMAGES 40

APPENDIX A-2: CULVERT GPR IMAGES 55

APPENDIX B-1: SPILLWAY SEISMIC REFRACTION PROFILES 72

APPENDIX B-2: CULVERT SEISMIC REFRACTION PROFILES 77

LIST OF FIGURES

- Figure 1. Location of Study area in Alaska 2
- Figure 2. View of the Spillway 4
- Figure 3. Stratigraphic sequence observed 10km northeast of study area 5
- Figure 4. Radar wave transmission 10
- Figure 5. CMP results 10
- Figure 6. Location of GPR and seismic lines in spillway 12
- Figure 7. Path of a critically refracted ray 13
- Figure 8. Seismic data plot 14
- Figure 9. T^2-X^2 plot of CMP survey points 16
- Figure 10. Before and after GPR images 18
- Figure 11. GPR line detail 19
- Figure 12. SIPWin© screenshot 20
- Figure 13. Two-layer seismic profile 21
- Figure 14. Three-layer seismic profile 22
- Figure 15. GPR image comparison and analysis 24
- Figure 16. Simple stratigraphic column 26
- Figure 17. Location of surveyed culverts 29
- Figure 18. Hyperbolae at culvert sites 32
- Figure 19: GPR image of culvert below one meter depth 34
- Figure 20. GPR image of culvert above one meter depth 34
- Figure 21. Culvert seismic profile 35

ABSTRACT:

Ground penetrating radar (GPR) and seismic refraction surveys conducted at a critical location on a glacial moraine near Yakutat, Alaska reveal its inferred stratigraphy. The moraine material observed from exposures and shallow excavation is composed of material ranging in size from medium sand to boulders >1m in diameter. Seismic data acquired on the moraine show a subsurface depth to refractor of ~10-15 meters. GPR images show events that reveal the stratigraphy to bedrock depth at 30m. The stratigraphy is like that seen at outcrops 10km northeast. With this interpretation, I produced a reasonable subsurface stratigraphy that identifies hydrogeologic units and depth to bedrock with one meter estimated resolution of depth (10%). The subsurface model provides valuable insight to potential stream incision during the next cyclical closure of Russell Fjord by Hubbard Glacier, the water body bordering the glacial moraine to the north. Based on the sediment depth, there does not appear to be any danger of them being scoured to bedrock.

GPR and seismic refraction surveys conducted at a different site, a Forest Service road near Petersburg, Alaska, help measure depth to bedrock and the water table. Data collected at several culvert sites show classic hyperbolic response from the GPR in imaging cultural artifacts. Engineering plans of existing culverts provide known depths to reflectors allowing radar wave velocity to be derived at each location, promoting the calculation of accurate depth to reflectors.

PART I. HYDROGEOLOGIC UNIT CHARACTERIZATION ON A RECENTLY ACTIVE GLACIAL MORaine USING GROUND PENETRATING RADAR AND SEISMIC REFRACTION

Introduction

Purpose and Objective

Cyclical advances of the Hubbard Glacier and the resultant elevated water levels and hydraulic head of Russell Fjord threaten to flood the Situk River near Yakutat, Alaska (Figure 1). Sport and commercial fishing on the river is Yakutat's main industry. The response of groundwater in a glacial moraine, the southern boundary of the fjord, to the increased water pressure is not known. Ground penetrating radar (GPR) and seismic refraction surveys were conducted at the

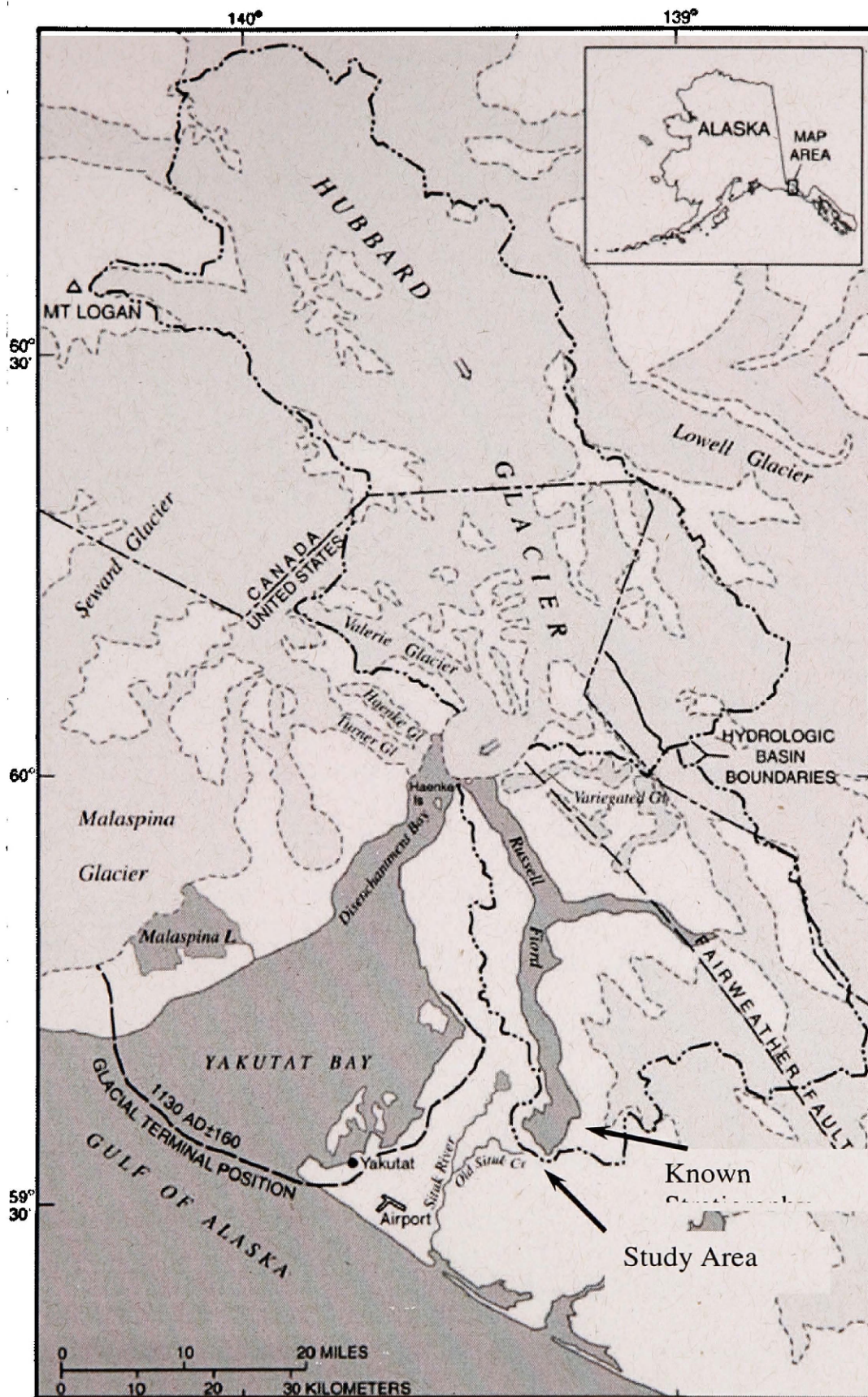


Figure 1. Location of study area and existing data with respect to their location in Alaska.

spillway through which the flooding would most likely occur to measure the depth to bedrock and the water table. The objective of this project is to identify hydrogeologic units of the moraine (composed of sand, gravel, cobbles, and boulders) to assist the Forest Service in qualitatively judging its response to changing hydrogeologic conditions associated with a cataclysmic flood.

Setting and description of the problem

The study area is a spillway (Figure 2) cut by water trapped within a late Holocene terminal moraine complex formed by Hubbard Glacier at the southern end of Russell Fjord (Barclay et al., 2001), and is on United States Forest Service (USFS) wilderness land within Tongass National Forest. The climate is temperate and precipitation exceeds 300cm per year. Judging from local observations and distant wells, the water table depth is guessed to be within five meters of the surface (USGS, 1995).

Uprooted trees on the moraine show underlying poorly sorted sediments that vary in size from coarse sand to boulders over one meter in diameter. No stratigraphic sections from previous studies are available at the exact location of the study area, but those described by King (1995) ten kilometers to the northeast (Figure 1) show horizontal beds of sandy gravel, fine sand and clay extending to bedrock about 21m beneath the surface (Figure 3).

The study area, being pristine wilderness and largely inaccessible, warrants subsurface exploration methods such as GPR and seismic refraction because they are non-invasive and portable. The dense forest growth is restrictive to GPR surveying in most areas, but there are areas that are clear enough to grant access. The seismic

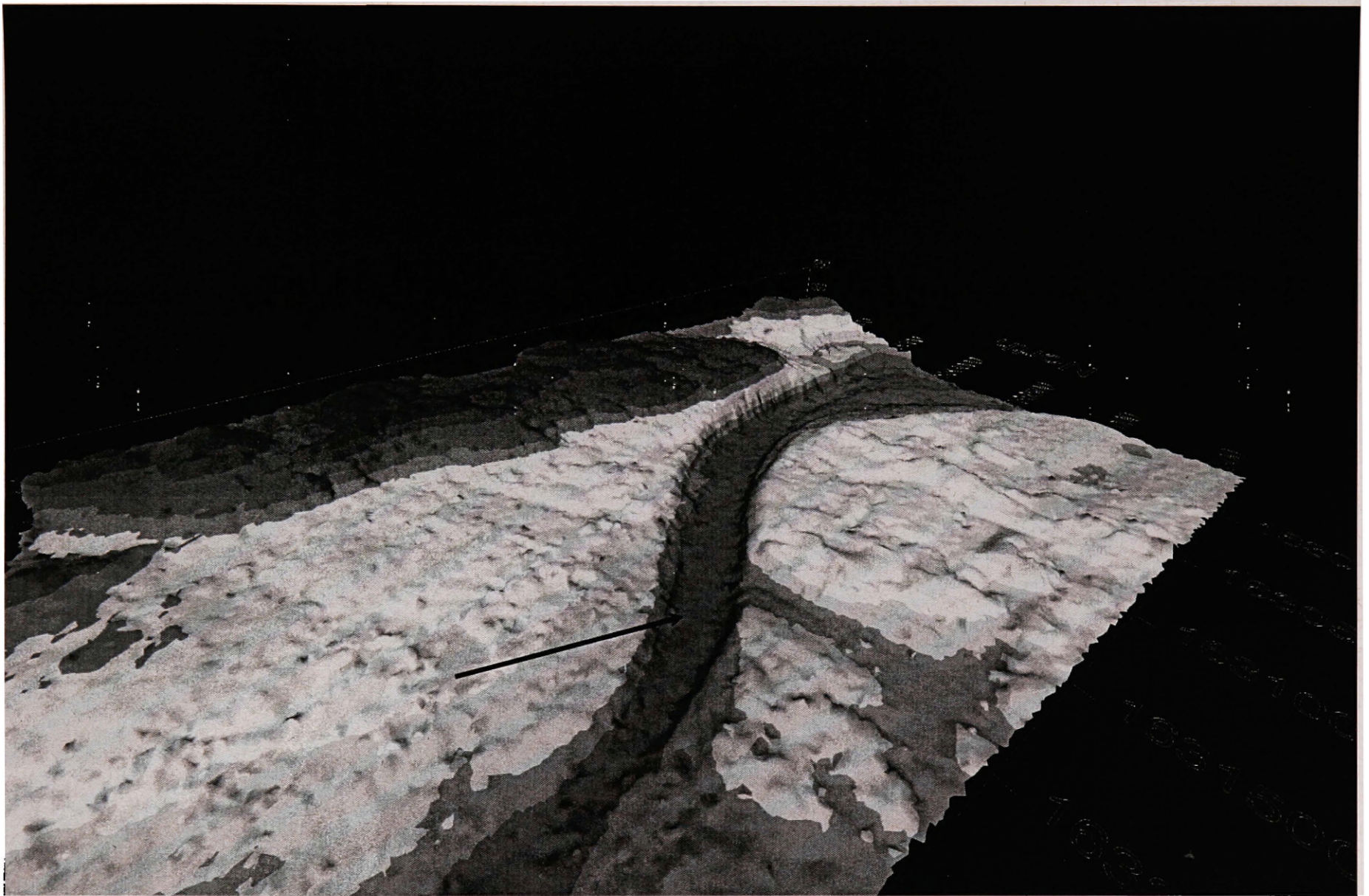
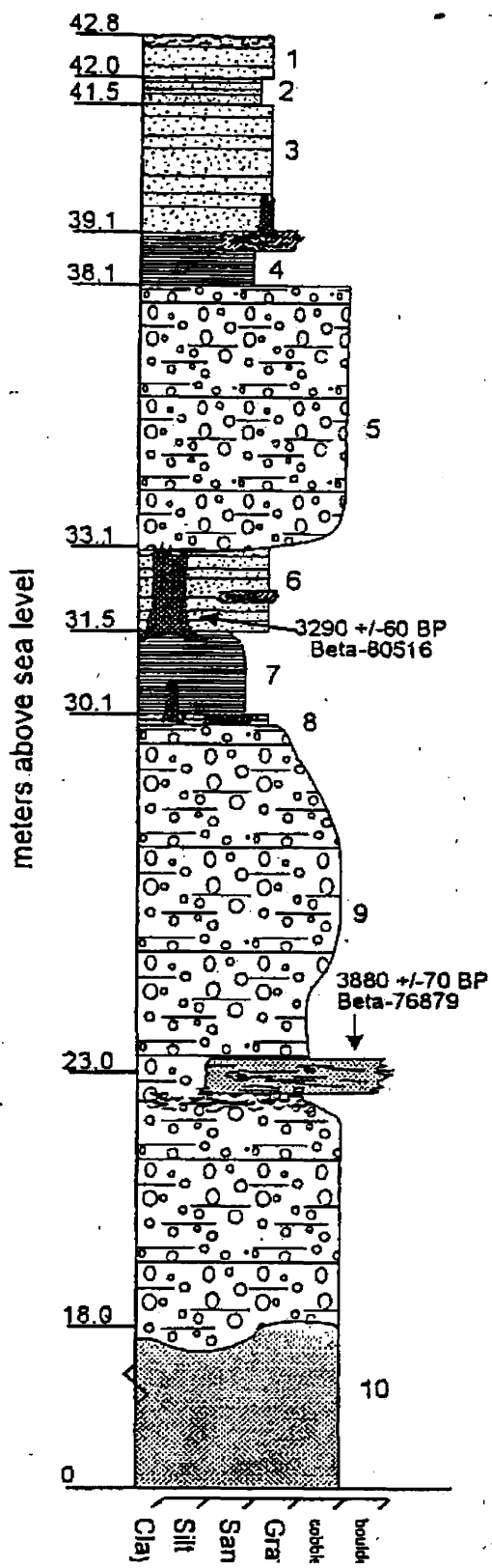


Figure 2. Study Area: Approximate location of GPR and Seismic surveys indicated by arrow. This spillway cut through a glacial moraine once carried impounded water northward (to right in picture) to Russell Fiord.



LEGEND

1. Modern soil developed at top of medium to coarse sand
2. Medium to fine sand with silt laminae and wood fragments
3. Sands with silt to pebble gravel interbeds
4. Horizontally bedded silts and fine sands. Lots of organic material including recumbent logs; one with a subfossil stump growing from it.
5. Stratified, well-rounded, cobble gravels with some thin sand beds. Truncates sands and in situ stumps below.
6. Medium to fine sand beds with silty laminae. Wood throughout with a major laterally continuous detritus layer near base.
7. Thin-bedded and laminated clay, silt, and sand. In situ stumps rooted in upper 50 cm.
8. Silty sand with organics, scattered wood detritus, and in places alder stumps.
9. Stratified medium sand to cobble gravel with interbeds of finer material. A thin (several cm) soil overlying an oxidized gravel horizon is present below a detrital wood layer with logs up to 53 cm dia. Also, in this zone are fine layers with very high organic black sand and gravel. A channel fill structure is present below this organic zone.

Figure 3. Stratigraphic sequence observed 10km northeast of study area. Modified from King, 1995.

survey was less affected by growth because the cabling can be routed around vegetation. The thick layer of forest litter proved a difficult medium in which to place geophones, a problem corrected with some minimal excavation (less than one liter).

GPR and seismic refraction are applicable to this study area because the materials of interest are close (<25m) to the surface, and because the subsurface is composed primarily of unconsolidated sediment. These two factors played heavily in the selection of antenna frequency for the GPR and geophone spacing along the seismic refraction survey lines.

Ground penetrating radar (GPR) has been used in a wide range of applications to locate subsurface artifacts and structure including depth to bedrock (Birkhead et al., 1996). In addition to locating water tables in push moraines (van Overmeeren, 1994), GPR has successfully imaged the extent and thickness of sediments beneath water bodies (Haeni et al., 1987). Surveys have also been conducted on an unconfined, heterogeneous and anisotropic glacial outwash aquifer composed of coarse to fine sands (Sandberg et al., 2002) to investigate the affect of features within this material on preferential groundwater flow. Shallow applications (<10m) of GPR in aquifer studies by Huggenberger, et al., 1994, Carreon-Freyre, et al., 2003, O'Neal and McGeary (2002), and Russell, et al., 2001, describe GPR as a tool for mapping structure and stratigraphy in unconsolidated sediments. Penetration depths by GPR can reach 21.3m with 80MHz antennas in coarse sand and gravel (Beres, et al., 1991). Based on previous work, the decision to use GPR on the shallow, saturated, horizontally bedded, unconsolidated sediments in the study area is a good one.

Seismic refraction is a reliable method for shallow subsurface analysis because seismic waves offer excellent penetration depth and resolution. It has been used to successfully image karst terrain and an underground tunnel in a shallow setting (Belfer, et al., 1998). Behera, et al., (2002) and Sain, et al., (2002) used seismic methods to map sediment structure in settings where sediments overlay bedrock. Ayers (1990) used seismic refraction on an atoll in Micronesia to identify freshwater lenses in an aquifer and characterize carbonate facies based on seismic velocity and classify unconsolidated sediment in the top-most layer. A shallow bedrock study by Pant and Murty (1981) explored the use of a hammer source and single channel time-recorder to quickly map the bedrock surface. Solution discontinuities in the Great Barrier Reef Province in Australia by Harvey (1977) show its use in identifying subsurface structure. Burke (1973) discusses the use of seismic refraction to map the thickness of Quaternary deposits in a shallow setting. The geologic setting at the moraine near Yakutat displays all of these characteristics, and seismic refraction is applicable for this investigation.

Methods

Ground Penetrating Radar

GPR measures the contrast in dielectric properties of the subsurface through which transmitted electromagnetic waves of a given frequency (radiowaves at 25MHz to 1GHz) travel. A portion of the wave's energy is reflected and absorbed, with the rest being transmitted at media interfaces with different dielectric constants. The

GPR control unit records the strength and two-way travel time of reflected waves and typically plots these as wiggle traces (Reynolds, 1997).

In general, greater image resolution is obtained with higher frequency (500MHz – 1GHz) antennas and greater depth penetration with lower frequency (25MHz – 50MHz) antennas (van Overmeeren, 1994). I used 50 MHz unshielded antennas because the depth to bedrock is thought to be ~25m in depth (King, 1995).

Radiowaves lose energy in a number of ways. Absorption from heat loss, and losses due to spreading are inherent within the system and cannot be removed by careful survey planning. Spreading occurs as radiowaves spherically diverge, and the energy per unit area decreases at a rate of $1/r^2$ (Reynolds, 1997), where r is the distance traveled by the wave. Geologic materials with low dielectric constants allow GPR to pass through unimpeded, and those with high dielectric constants can attenuate or block the signal entirely. Large contrast in this property creates strong reflections. While this is the primary way of identifying subsurface features, it also serves to reduce signal strength. Objects with dimensions similar to the signal's wavelength provide no common planar surface against which the wave can reflect, and cause attenuation known as *Mei* scattering, sending reflections in multiple directions resulting in a noisy radar image. The wavelength is the product of the pulse period of the antennas and the velocity of the medium (Reynolds, 1997). The electric properties of a material also influence wave attenuation. Materials with high conductivity such as clay absorb wave energy and increase signal attenuation, prohibiting further penetration (Reynolds, 1997).

GPR records reflections measured in two-way travel time along a survey line. Deriving the GPR wave velocity allows conversion of travel time to depth and thus construction of subsurface stratigraphic models. Wave velocity in a subsurface medium is the speed of light (in free space), divided by properties of the material, as described by the following equation:

$$V = c / \{(\epsilon\mu / 2) [1+P^2] + 1\}^{1/2}$$

where:

V = velocity (m/s)

c = speed of light in free space (m/s)

ϵ = relative dielectric constant

μ = relative magnetic permeability

P = loss factor (Reynolds, 1997).

In practice theoretical or lab-determined velocities don't work well; empirical determinations are best.

One common field experiment used to determine velocity is the common mid-point (CMP) method. As distance between transmitting and receiving antennas is increased, the two-way travel time to a particular reflector also increases. The result on a radar image is a hyperbola (Figure 4). This makes for convenient velocity analysis, as the most visible reflectors can be used. Nakashima, et al., (2001) describe using CMP surveys to calculate the dielectric properties and derive velocities for multiple layers in the subsurface from hyperbolae in GPR images. A plot of T^2 vs. X^2 linearizes the hyperbolic data, and the slope of a best-fit line yields the squared wave velocity (Beres, et al., 1991). My execution of the CMP survey lines took place

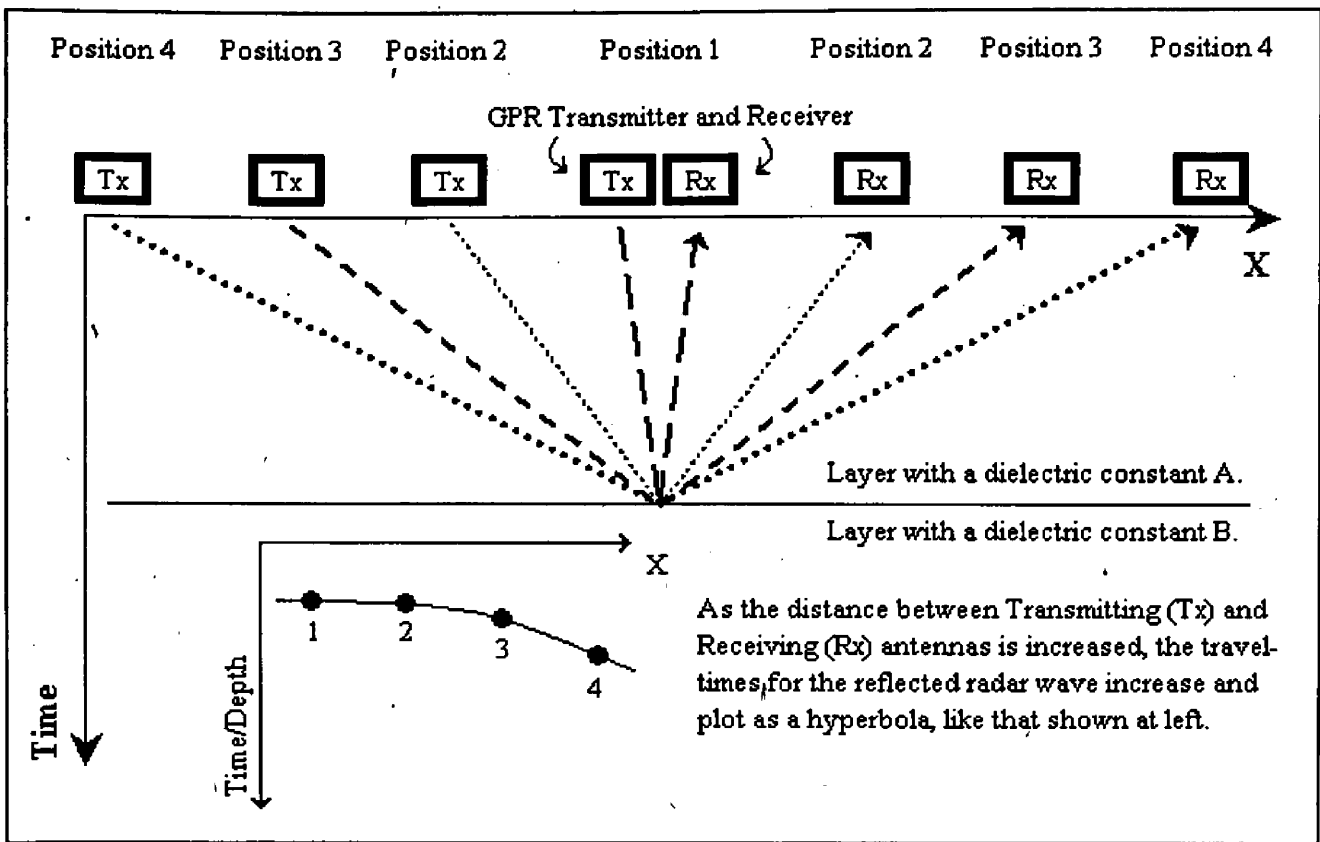


Figure 4. Sketch describing the transmission of radar waves between GPR transmitting and receiving antennas during a CMP survey. Picture also shows a simplified plot reflecting longer travel times with increasing antenna separation.

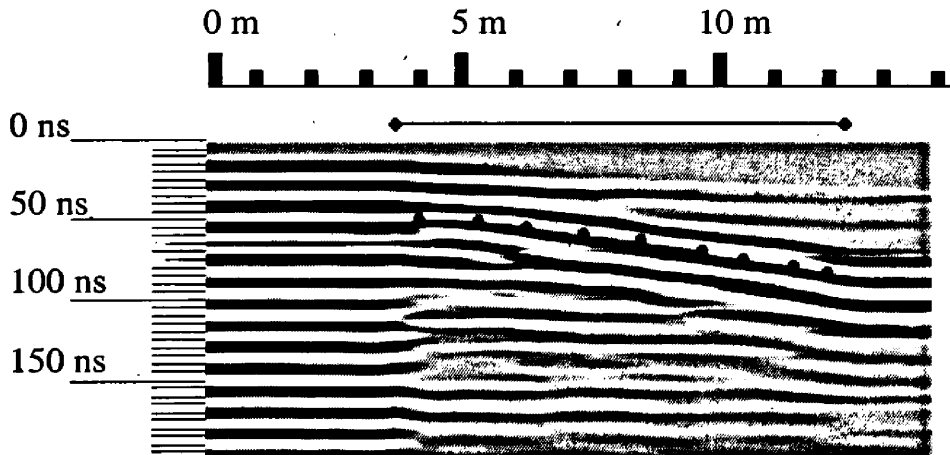


Figure 5. Results from one common mid-point (CMP) survey, Line 18C, executed in the spillway with points chosen along a reflector for velocity analysis. The line segment indicates the period during which the antenna separation was occurring. Filters used: DC Offset Removal (102), Band Pass (Upper: 140, Lower: 35), Time Varying Gain (Start: 102, Linear: 100, Exponential: 3).

in a grassy field somewhat removed from the most dense concentration of survey lines. Two field personnel moved the antennas away from a common mid-point at a constant rate while the GPR collected traces at a rate of 4Hz. Figure 5 shows a representative image obtained with CMP surveying.

I used a MALA Geoscience RAMAC GPR system, and their Groundvision[®] v.1.3.6 software to record and process the data. Groundvision[®] v.1.3.6 is a user-friendly graphical user interface that allows the surveyor to adjust the GPR settings to collect data in a manner applicable to the study area, and antenna frequencies used. I used a Time Window setting of 1557ns to record reflection events within that time period, and the Sampling Frequency was 1163MHz. I collected traces along the survey lines at 0.1-meter intervals, and the antenna separation (common-offset) was two meters.

I chose the location of the survey lines by examining topographic data generated from ground-based and LIDAR surveys performed in 2002 by the USFS (Figure 6). The data reveal the shape of the study area and provide elevation constraints for calculating bedrock and subsurface feature elevation. The topography is relatively level in the spillway (slope < 0.2%), but the thick vegetative groundcover and dense Sitka spruce groves proved exceedingly prohibitive to the GPR system's fiber optic cables, making it difficult to survey long, unbroken lines. As a result, 12 lines varying from 10-40m make up the GPR data set.

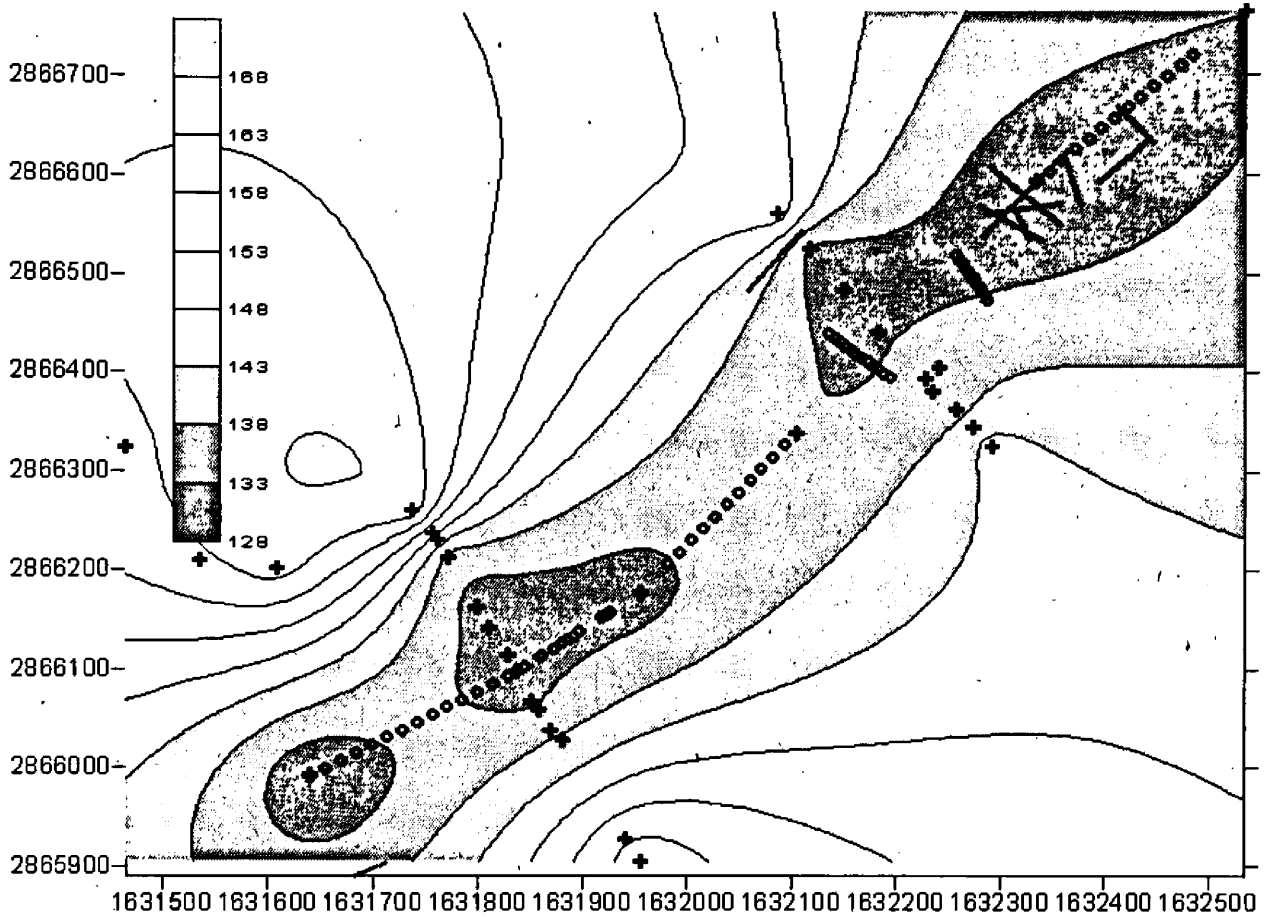


Figure 6. Location of GPR and Seismic survey lines in study area. Solid black lines represent GPR and circle-lines represent seismic surveys (numbered). The contours show elevation (dark = low elevation). The axes are labeled with northing and easting values in the NAD 27 coordinate system.

Seismic Refraction

Seismic refraction exploration exploits bending of seismic rays at velocity interfaces. Snell's law governs the geometry of the travel path and standard techniques allow for recovery of layer velocities and depths to those layers. To collect the seismic waves, geophones evenly spaced from the seismic source recorded

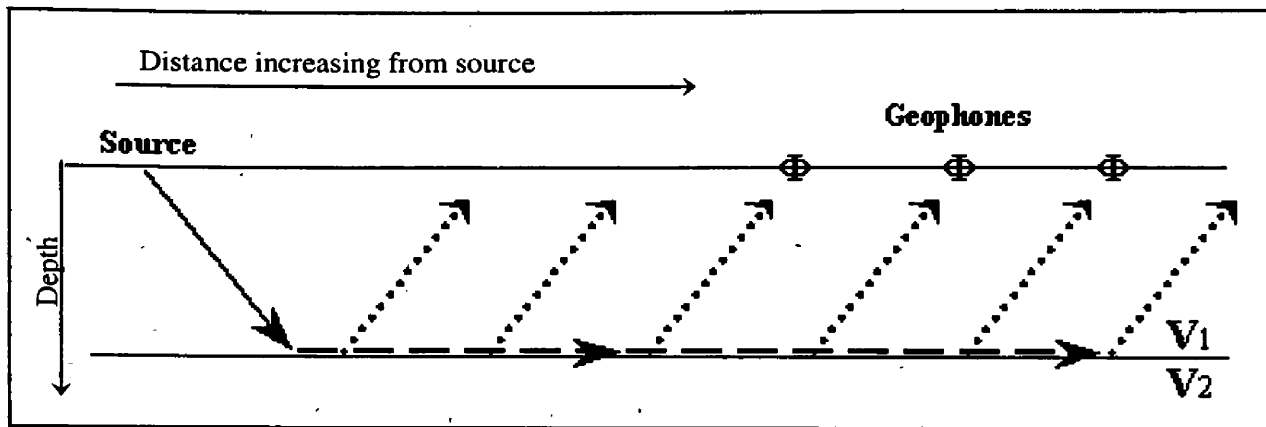


Figure 7. Depiction of a critically refracted ray.

the arrivals of p-waves returning to the surface. Increasing the distance between source and receivers and increasing the source signal strength increases the effective depth of resolution obtained with a seismic survey. The path of a critically refracted wave is generalized in Figure 7. Processing the data requires choosing the first arrival of the signal at each geophone, and plotting the time (t) taken from source to geophone versus the distance (x) the wave traveled. The inverse slope of the t - x plot is the velocity of the seismic wave through the higher-velocity layer overlain by the slower layer (Fig 8). I collected forward and reverse shot data as standard procedure to test for asymmetric travel times and lateral velocity changes as well as any dip of the refractors.

We used a Geometrics SmartSeisSE 12-channel seismograph to collect seismic refraction data. Geophone spacing ranged from 1.5 - 5m, according to

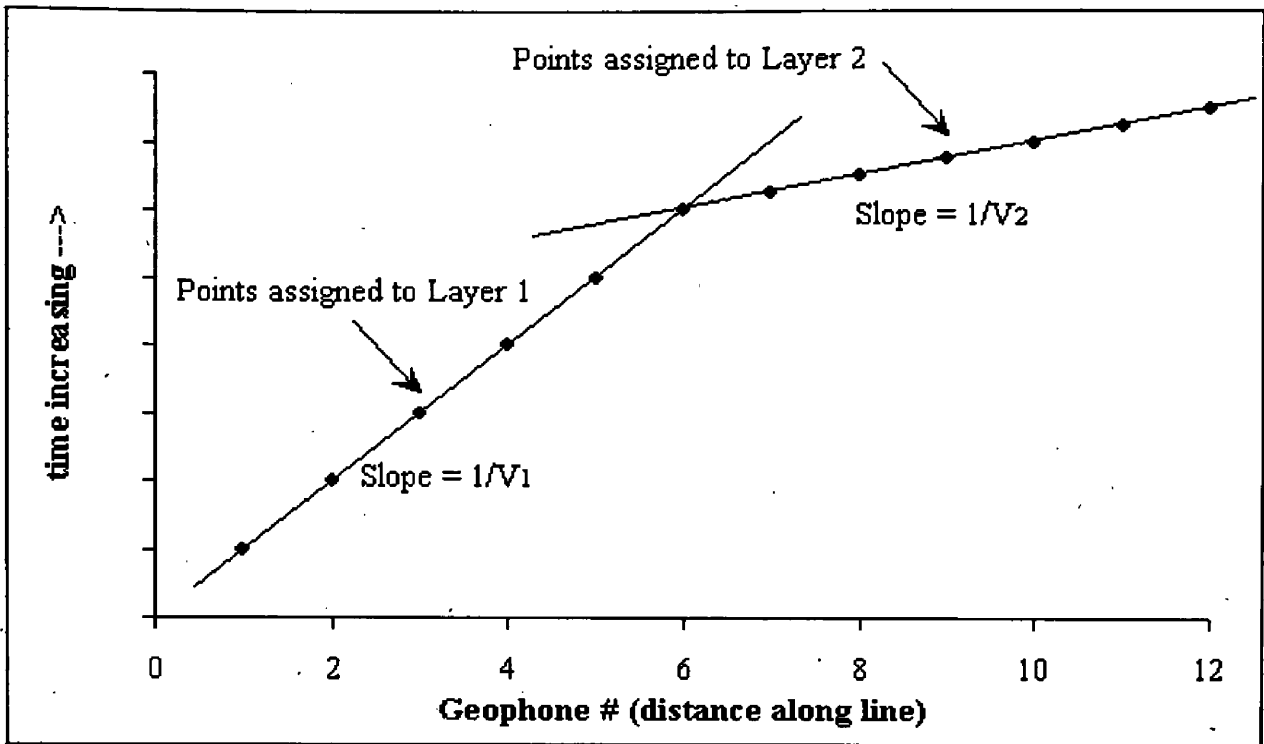


Figure 8. Example of seismic data t-x plot for the two-layer case. The inverse slopes of the best-fit lines yield velocity of the upper layer (steeper slope) and second layer.

available space in the study area. Shotpoints (created with a sledgehammer and an aluminum baseplate) also fell in the same area where the topography is relatively flat. Figure 6 shows the location of the seismic survey lines. Use of this method assumes velocity increases with depth. Collecting refraction data on the generally flat topography of the spillway floor eliminated the need for topographical corrections to the data. Data processing was expedited using SIP[®] software (Sipwin[®]) from Rimrock Geophysics. SIP[®] allows the user to input multiple spreads, source shot locations, and reverse lines. Data collected from shots performed at both ends of each line allowed SIP[®] to calculate the geometry of shallowly (< 10°) dipping layers.

Results

GPR: CMP and Common-offset Survey lines in the Study Area

The raw GPR images are processed with a series of filtering and gain functions in Groundvision[®] to improve the resolution of the radar images. The reflection events were strong, and required little enhancement by filtering. Of the seven available tools, only a DC filter, Band Pass filter, and Time Varying Gain were used to clarify the images (App. A-1,2). Filtering out the DC component removes the constant offset in the data. The Time Varying Gain uses a function of time (two-way travel time of a radar wave) to amplify the features in the radar image that are weak due to absorption and attenuation caused by subsurface properties as travel time increases.

Band Pass filtering removes high- and low-end background noise from the wave traces. Among this noise is “wow,” a low frequency noise component that is a caused by the GPR unit (Gerlitz; et al., 1993). Other sources of noise include power lines, cellular phones, and the notebook computer used to record GPR data traces (Olhoeft, 2000). All of these have an electromagnetic signature at varying frequencies that contribute distortion to a GPR image. Ringing caused by ground-coupling of the antennas with the surface (Reynolds, 1997) causes the alternate black and white banding that is found in all the GPR images. Typically, the appropriate pass band is centered on the main antenna frequency with frequencies above and below main antennae components filtered out. I chose to use the automatic setting controls for Groundvision[®]'s Band Pass and Time Varying Gain tools because doing

distance vs. time, slope=velocity

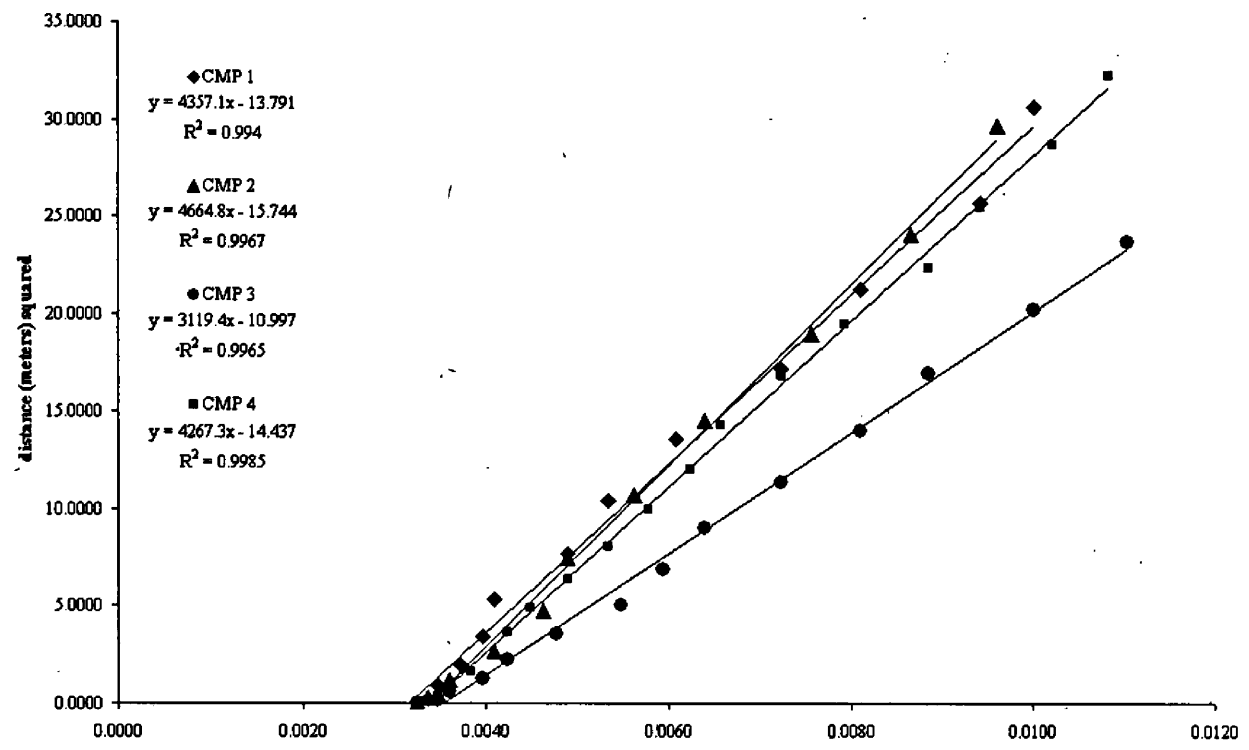


Figure 9. T² vs. X² plot of points taken from CMP surveys.

so brought out the three separate events common to each radar image relatively well. However, the start sample for the DC correction and the Time Varying Gain were set manually.

Figure 9 shows the T²-X² plots of point-values taken from all four CMP gathers. The average velocity derived with this method is 64m/μs with a standard deviation of 5.5μs/m. I used this average velocity to calibrate the radar images in Groundvision[®] and resolve the depth to reflection events along the GPR survey lines.

Figure 10 shows the before and after filtering images of GPR Lines 7 and 10. These images are representative of the data returned from most of the lines surveyed in the spillway (Appendix A-1). Most of the images show numerous reflections in the first few meters of signal transmission, followed by a marked absence of reflections beneath 10m. A sudden, strong reflection event is shown in all of the images near 30m. The shape and location of this reflector is consistent through several of the images and is most likely from bedrock. The beginning of Line 7 is nearly coincident with the end of Line 10 in the field (Inset, Figure 9) and the radar images show the bedrock reflector at the same depth at this location. Other instances where GPR lines approach or cross one another also show the same depth to the bedrock reflector. A detailed image of the GPR line orientation appears in Figure 11.

Seismic Images

Plotting user-picked first-arrival times of the seismic signal from each geophone (Figure 12) allows layer assignments from t-x plots of the input data. SIP[®] calculates depths and velocities with an inversion algorithm. It uses least squares to compute velocities, the delay-time method (Reynolds, 1997) to estimate depths, and follows with three iterations of ray tracing from the source to each geophone, comparing their travel times to those recorded in the field. It then adjusts model depths to minimize the difference between computed and measured travel times. This assumes a two-layer case with velocity increasing with depth. For additional layers, SIP[®] repeats the process ignoring the overlying layer used in the previous calculation.

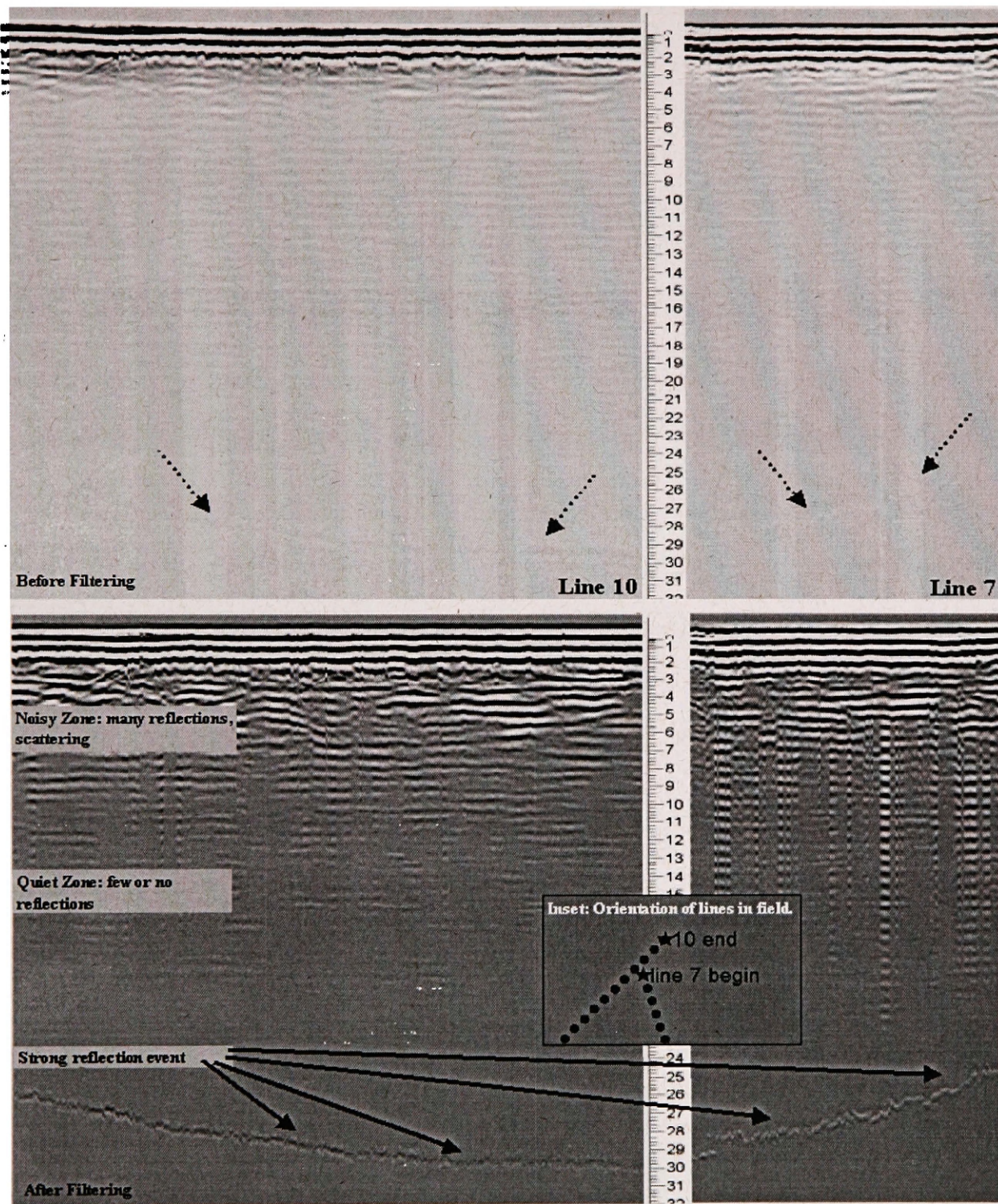


Figure 10. GPR images shown before (top) and after (bottom) processing. Scale is 1:1 and shows depth in meters. Filters used: DC Offset Removal (107), Band Pass (Upper: 140, Lower: 35), Time Varying Gain (Start: 107, Linear: 100, Exponential: 1).

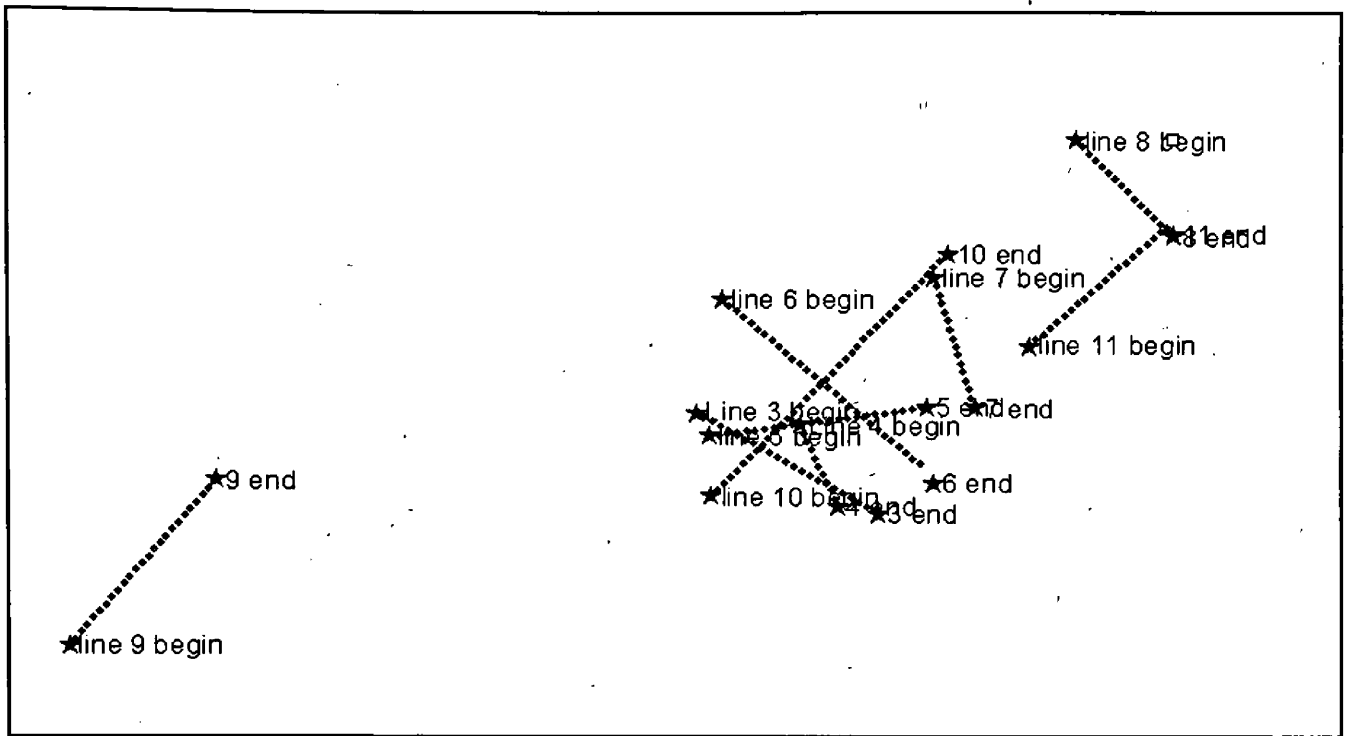


Figure 11. GPR Lines as they are located in the study area. Line 10 is 37 meters in length.

For example, instead of tracing the rays critically refracted along the interface of Layers 1 and 2, it traces those along the boundary between Layers 2 and 3, et cetera.

Images created with SIP[®] software consistently show refraction between layers with high contrasting p-wave velocity at a depth around 15m (Figure 13). This result is common among the seismic lines surveyed in the spillway. Two of the geophone spreads were long enough to give reasonable travel times to derive a three-layer solution. Figure 14 shows the location of refractors in each of these profiles.

SIP[®] software generated Profile A in Figure 14 from three forward shots only

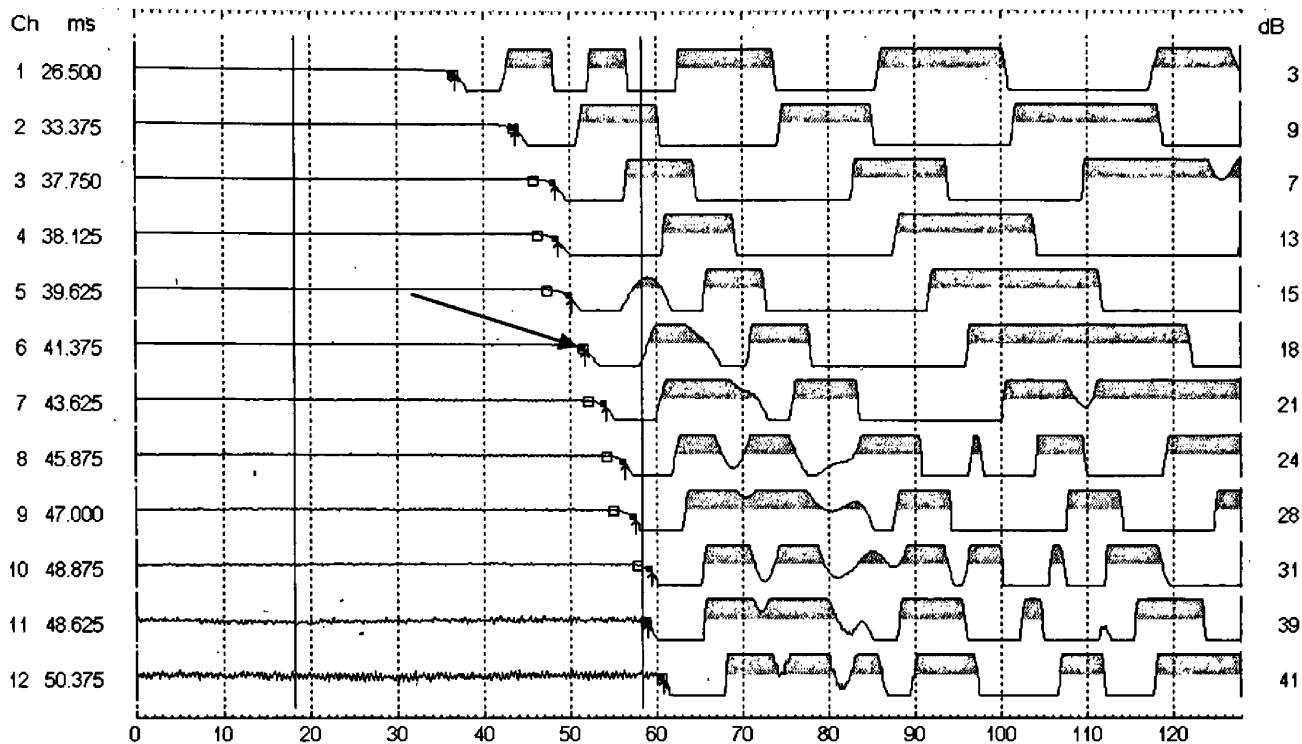


Figure 12. Screenshot from Sipwin[®] software when making first arrival picks (shown by arrow). The traces are shown clipped and shaded to provide clarity in the image. Channels (geophones) are numbered at the left with pick-times (in ms). Numbers at right show the gain level of a particular channel.

(reverse lines were aborted in the field). Details regarding survey geometry (geophone spacing, locations, etc.) are found in Appendix B-1.

Image Interpretation and Discussion of Derived Subsurface Properties

The advantage of using both GPR and seismic refraction surveys is the ability to provide evidence supporting the findings of each survey. The seismic refraction surveys provide depth to refractors. Seismic velocities are indicative of certain environments and good guesses of composition are possible. The GPR uses different

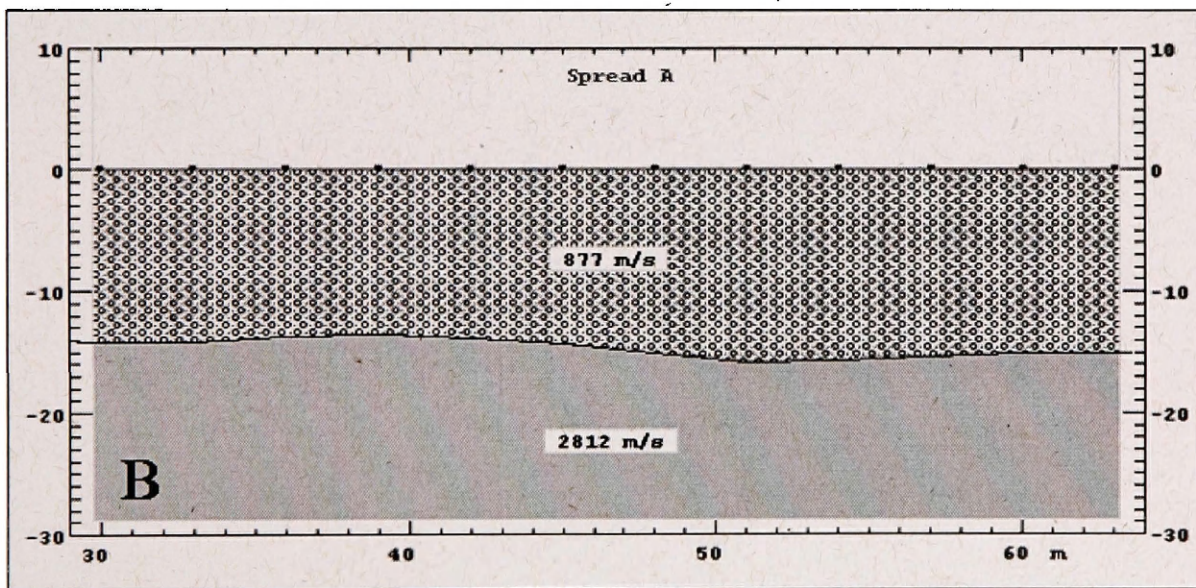
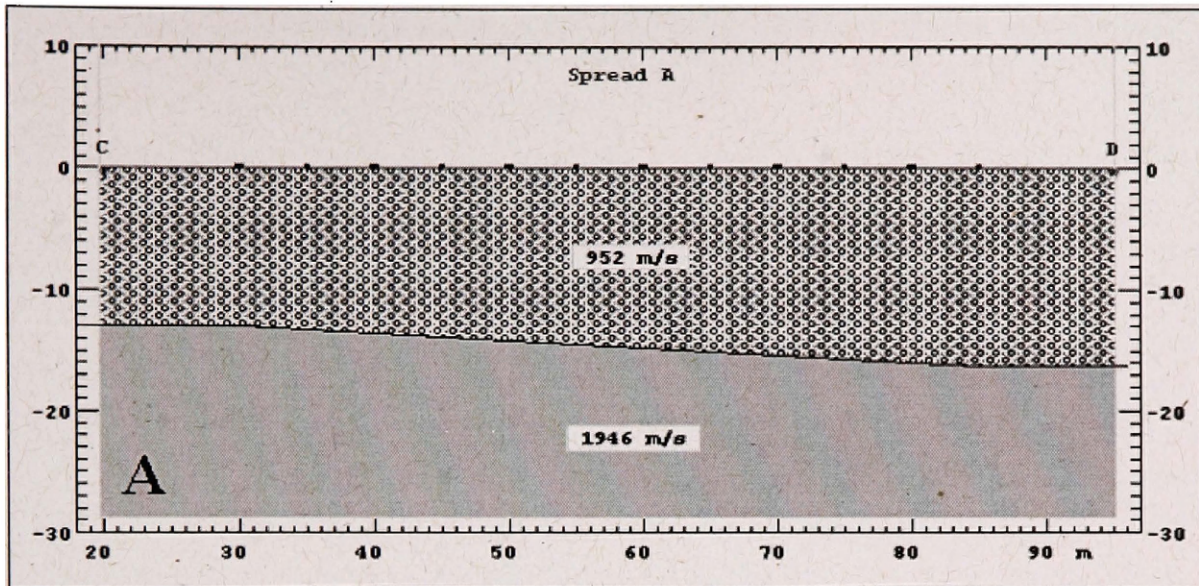


Figure 13. Two-layer profiles created with Sipwin[®] with the inversion algorithm showing a refractor about 15 meters deep. Profiles A and Profile B are Seismic Lines 6 and 2, respectively (Fig. 5).

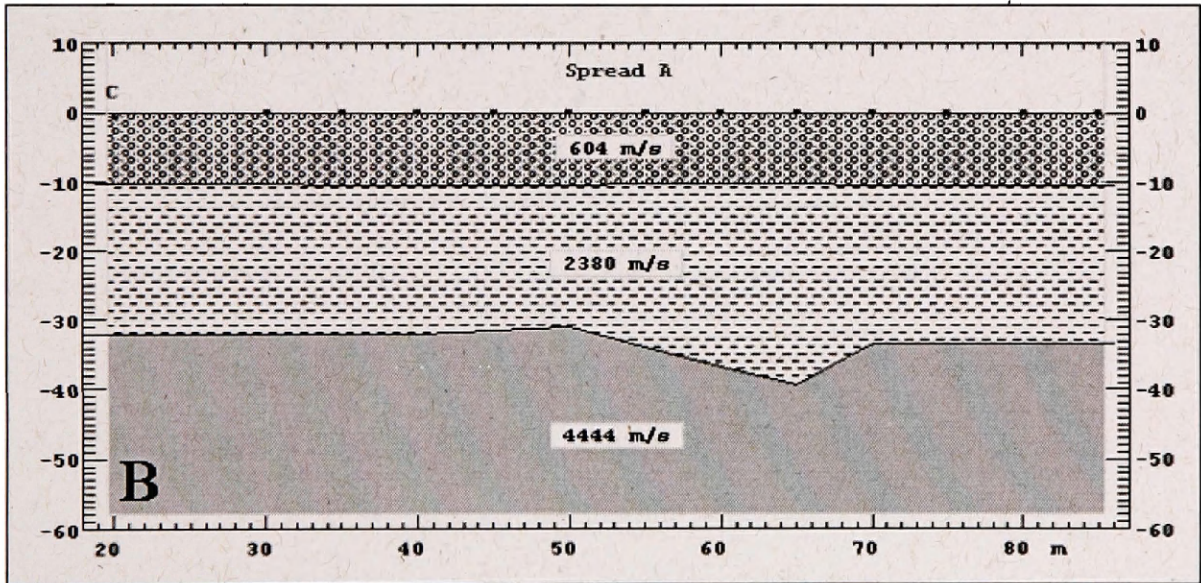
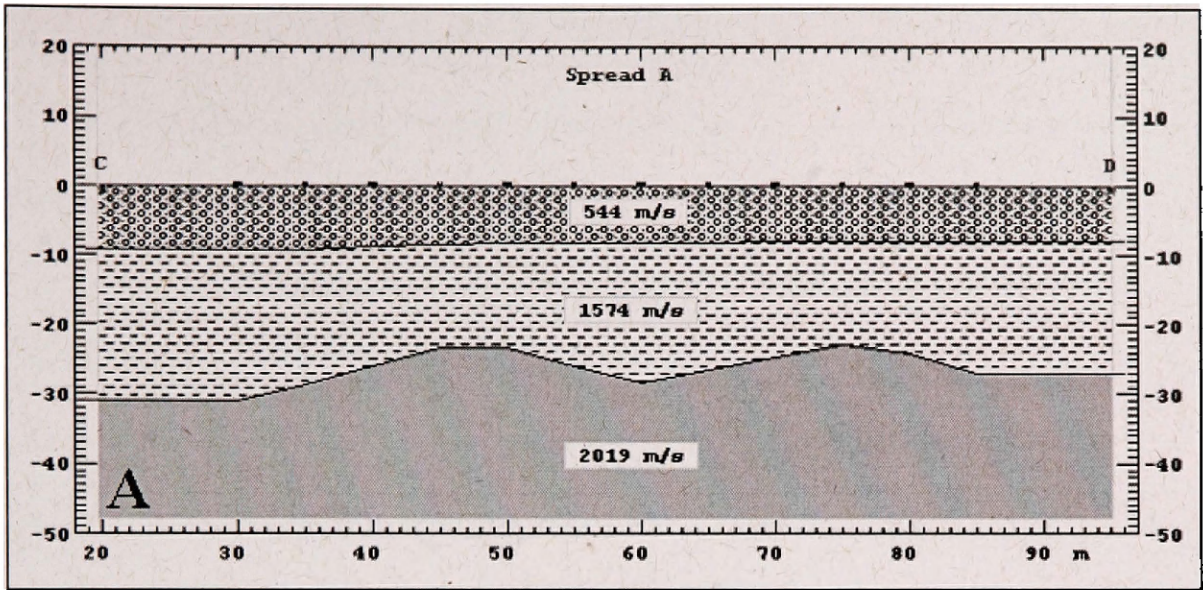


Figure 14.. Three-layer profiles created with Sipwin[®] with the inversion algorithm showing refractors about 10 and 30 meters deep in both cases. Profiles A and Profile B are Seismic Lines 3 and 1, respectively (Fig. 5).

material properties that lead to a determination of the layer's composition and, provided a reasonable velocity can be assumed or derived, estimates of depth are represented on GPR images. Together, they tell a more complete story than either could alone.

Three distinct events are visible in images from the GPR data. Hyperbolae and noisy scattering are shown in the topmost region of the radar images to 10 meters depth, indicative of objects in the subsurface on the same order of magnitude in size to the signal wavelength (Figure 15)(Reynolds, 1997). Using the average velocity (64m/ μ s) found with CMP surveying, the wavelength is 1.28m. This suggests a layer comprised of large cobbles to boulders on this order of size, and is consistent with rocks observed at the surface.

There are few if any radar reflections appearing beneath the topmost noisy zone in Figure 15. This quiet zone suggests signal attenuation upon contact with a conductive layer, which is most likely rich in clay. Clay is a known conductor and absorbs wave energy, resulting in a weaker signal propagating further into the substrate. There is no clear location of this attenuating layer, but the signal is markedly weaker beneath 10m in depth.

Images generated from three-layer seismic refraction data show a refractor occurring at about this same depth, 10 meters (Figure 14). The velocities of each upper layer are <1000m/s, and the velocity of the next lower layer range from 1500-2800m/s. These velocities are within acceptable ranges for near-surface sand and gravels and clay bodies (Reynolds, 1997).

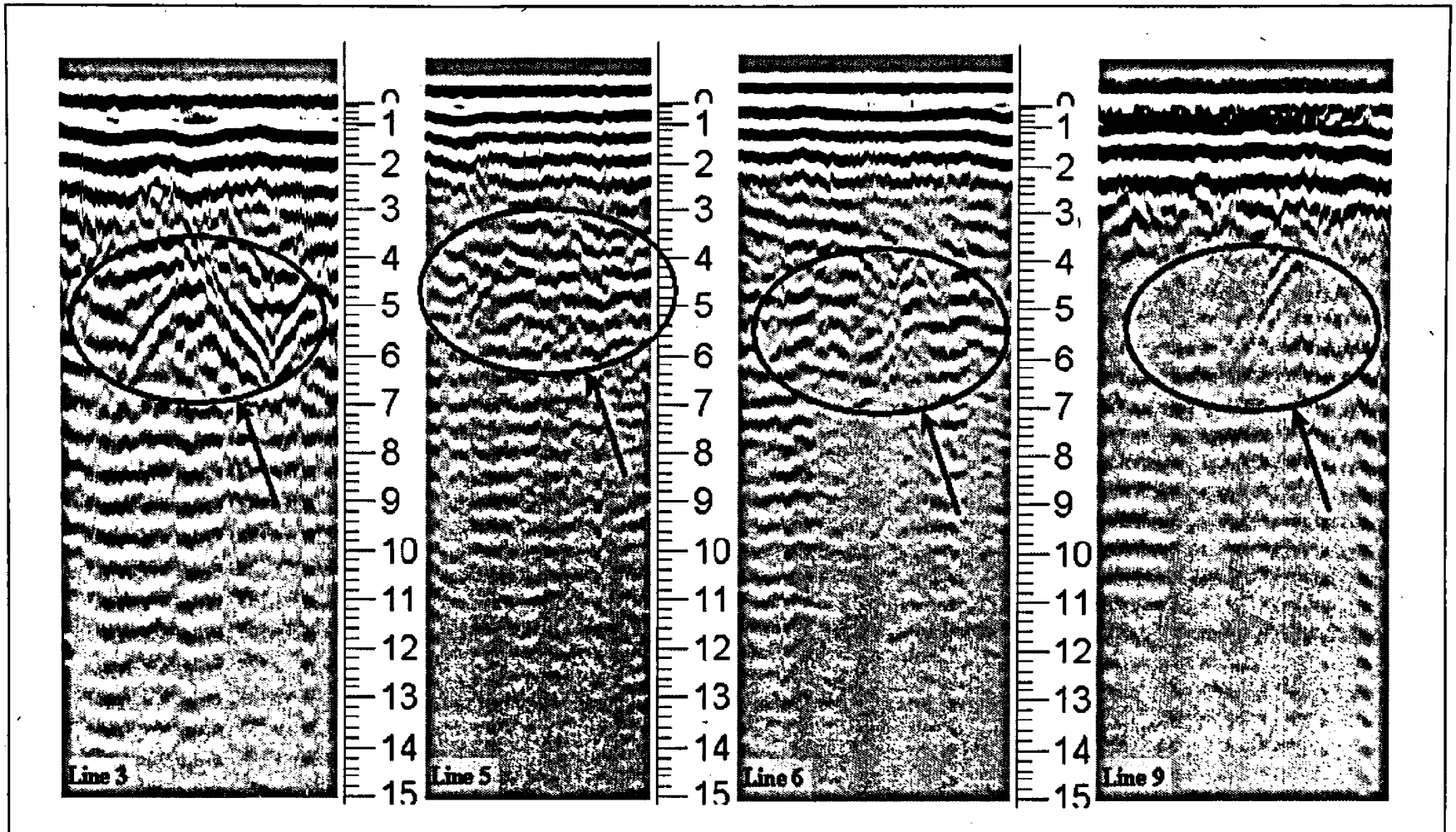


Figure 15. Depth to 15 meters showing noisy zone (indicated by arrows) composed of sediments with sizes approaching the GPR signal wavelength (from left to right: Line 3, Line 5, Line 6, Line 9). Scale is 1:1. Filters used: DC Offset Removal (107), Band Pass (Upper: 140, Lower: 35), Time Varying Gain (Start: 107, Linear: 100, Exponential: 1).

A strong radar reflection event occurred in each survey line around 30m depth in spite of signal scattering attributed to the top-most layer of sediment, and the unknown degree of signal absorption caused by the apparent presence of a clay-bearing layer. The most likely interpretation is bedrock at around 30m depth. The agreement between the GPR images shows lateral continuity of the strong bedrock reflection, both in the area of high survey concentration and at those survey lines farther west and south of the concentration. Considering the climate and the one-meter change in elevation of the reflector over distances less than 40 meters, the reflection occurring as result of interaction with the water table can be ruled out; the dip is too deep and steep to be the water table. The water table is within the first few meters, and cannot be seen on the GPR images because it is within the ground-coupling zone.

The data from the seismic spreads long enough to show a three-layer case include a refractor around 30m in depth. The velocities derived from that application of the data for the third layer are 2019m/s and 4,444m/s, a reasonable value for bedrock velocity. Thus both radar and seismic refraction show bedrock at about 30 meters.

A topmost layer of sediments ranging in size from sand to boulders, overlying a clay-bearing layer, above more unconsolidated material that overlies bedrock is the general sequence found with the GPR and seismic surveys. This same general pattern is shown at the exposure to the northeast (King, 1995). Comparing a simple stratigraphic column created from the moraine data (Figure 16) and the strat-column put forth by King shows the similarities between the two. Therefore, I suggest the style of the stratigraphy is laterally continuous from the site 10km northeast of the

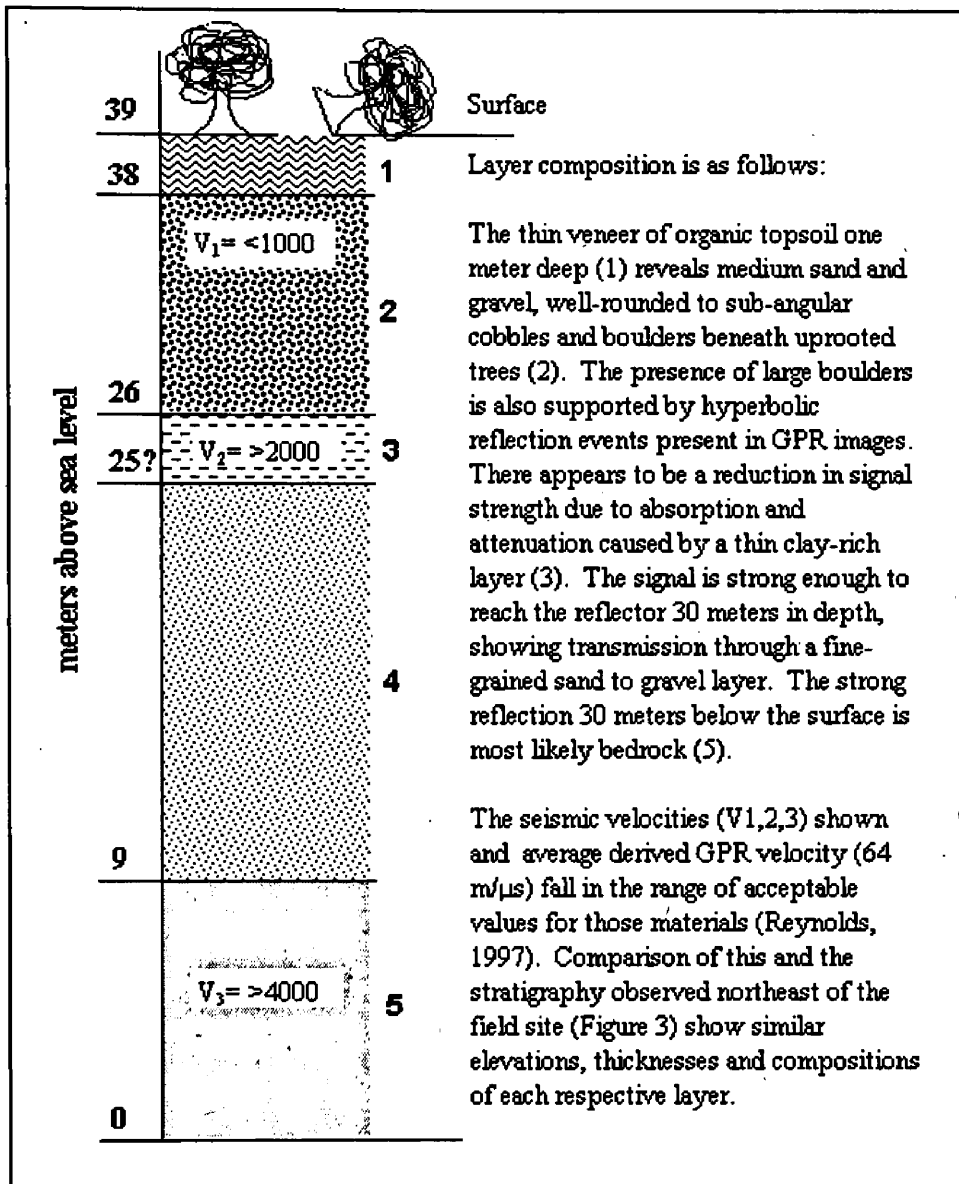


Figure 16. Simple stratigraphic column showing seismic and GPR velocities in each layer.

study area through the spillway itself. Most likely, the same glacial and fluvial processes that formed the sequence to the northeast deposited the spillway material. The three GPR events in each image provide evidence of this, and are supported by the seismic data that suggest refraction in the vicinity of the attenuating clay-bearing layer and provide derived seismic velocities of the clay-bearing layer and the unconsolidated sediments above it. The 3-layer seismic data also show a refractor in the same place as the strong bedrock reflection in the GPR images. Furthermore, this study shows the utility of using two geophysical methods to increase the ability to interpret the structure and properties of the subsurface.

PART II. LOCATING BEDROCK SURFACES IN AREAS WITH KNOWN FEATURES USING GROUND PENETRATING RADAR AND SEISMIC REFRACTION

Introduction

The Tongass National Forest has been implementing a culvert replacement program to improve fish passage on the Forest. One project located on Mitkoff Island, Alaska, replaced culverts installed in the 1980's to create streamlike conditions beneath Forest Service roads. These new culverts occupy more space than the originals requiring excavation for their installation. The USFS asked me to determine the depth to bedrock at culvert sites to estimate the amount of material that needed to be removed, and therefore provide a method by which to better estimate costs associated with each site. Given that the USFS was going to excavate where we surveyed the profiles, I was presented with an ideal situation in which to get some "excavation truth" after collecting GPR data.

The culvert sites are situated at five locations stretched along Forest Service Road #6245, Mitkoff Island (Figure 17). The crown of the road constructed over the culverts is composed of unconsolidated silt, sand, and gravel, containing larger rocks up to 0.5m in diameter. Depth to the culverts is known at each survey site, and ranges from one-half to about 2.5 meters' depth below the road.

There are numerous culvert locations that do not serve as adequate fish passage sites in Tongass National Forest and their replacement requires the expenditure of vast resources. In order to properly budget and appropriate funds to

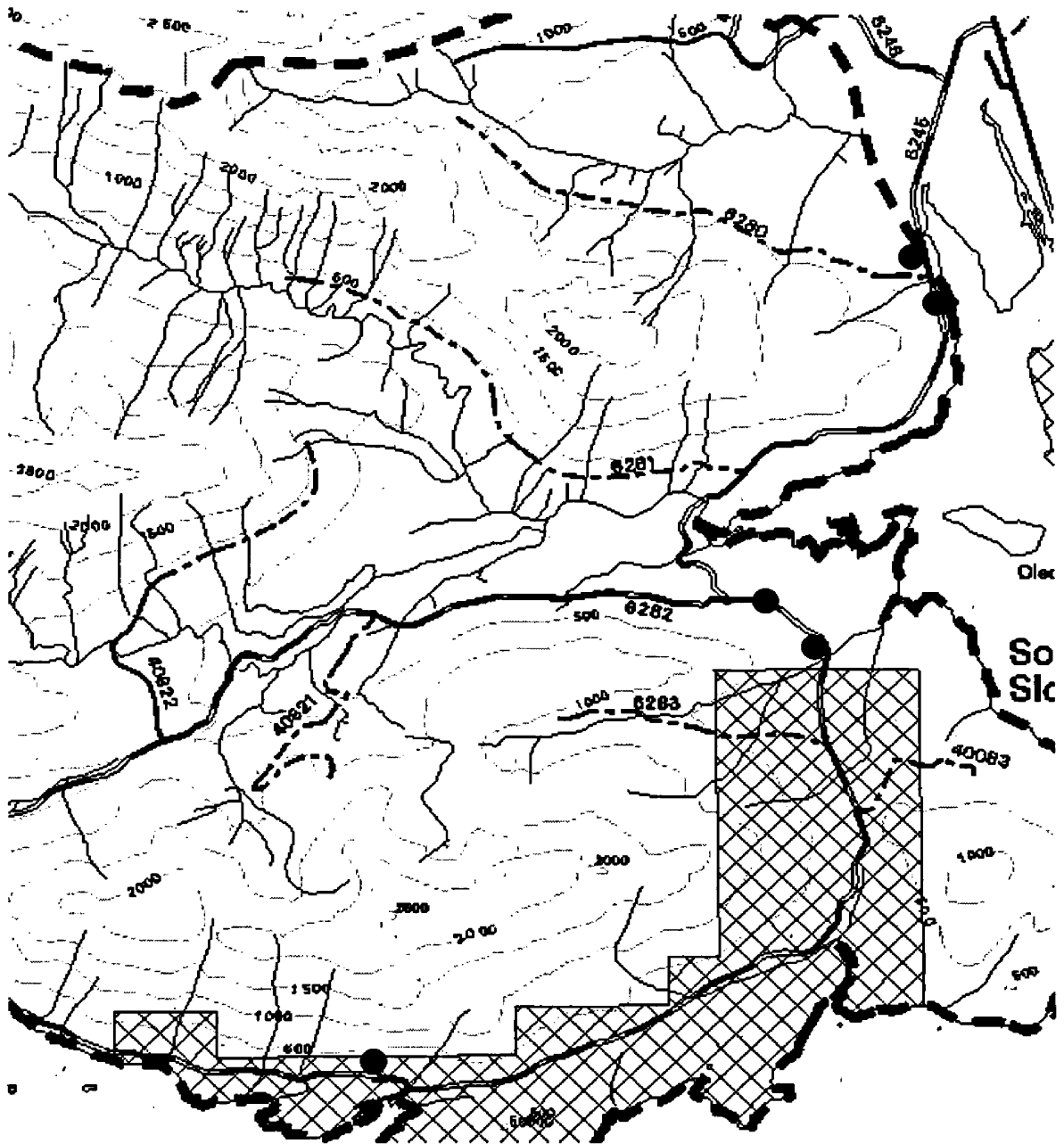


Figure 17. Map of Southern Mitkoff Island showing culvert site survey locations.

these projects, a better understanding of the cost accrued by excavation of bedrock is needed. The cost per unit of excavated bedrock is considerably greater than that of unconsolidated sediment. Observations of streambeds and exposures near the culvert sites promote the assumption of bedrock depth to be >10 meters at each location. The

objective of these surveys is to collect data with both GPR and seismic refraction inexpensively and non-invasively to resolve depth to bedrock, to assist the Forest Service in estimating excavation volume.

Methods

The methods and equipment described earlier for the glacial moraine surveys are generally the same as those applied to the culvert sites.

I chose 100MHz radar antennas to achieve better resolution at the expense of depth because the target depth was less than 10m. Nakashima, et al., (2001) and van Overmeeren (1994) show resolution to 10m with GPR on glacial push moraine deposits and unconsolidated sediments, respectively. Executing common mid-point surveys was not necessary at the culvert locations because the known depths to the existing culverts make it a simple task to calculate velocity from two-way travel times.

I collected traces along three parallel GPR lines at 0.1m intervals. Each line is 20m long and runs east to west; the lines are separated by about three meters. Seismic refraction lines were established on both edges of the road across the culvert and on both east and west sides of the culvert to collect data that were not influenced by the presence of the culvert. In most cases, geophone spacing was one meter, and shotpoints stepped away by increments of five meters. Geometry and locations of the seismic lines with respect to the culverts are given in Appendix B-2.

Results and Discussion

GPR data

Figure 18 shows the classic hyperbolic shape of an object with varying dielectric constant detected with the GPR as the unit approached the feature at Milepost 1.256. The velocity is found by taking the known depth to the top of the culvert and changing the velocity setting in Groundvision[®] until the depth on the image matches the known depth. Thus the depth in the figures is accurate. I repeated this process at each culvert location and found the velocity to be an average of 83μm/s with a standard deviation of 4.03m/μs.

Comparing the moraine and culvert surveys' velocities shows a discrepancy between the two areas. The areas are similar compositionally, and both are saturated (or at least wet). However, the unconsolidated sediments along the Forest Service road are mechanically compacted. Velocity tables (Reynolds, 1997) show higher velocities through homogeneous, igneous, non-porous rock, than those through unconsolidated material. Compacting the road materials reduces the amount of air and water in the material, making it more homogeneous and conducive to the propagation of radio waves.

Black and white banding at the top of each image is apparent in these GPR images just like in those collected at the moraine. This negates the ability to distinguish objects in the very shallow subsurface. Comparison of Figure 18, with Figure 19 at Milepost 4.962 reveals how ground-coupling interference hinders interpretation. The top of a 30-inch culvert at this location is apparent at a depth of

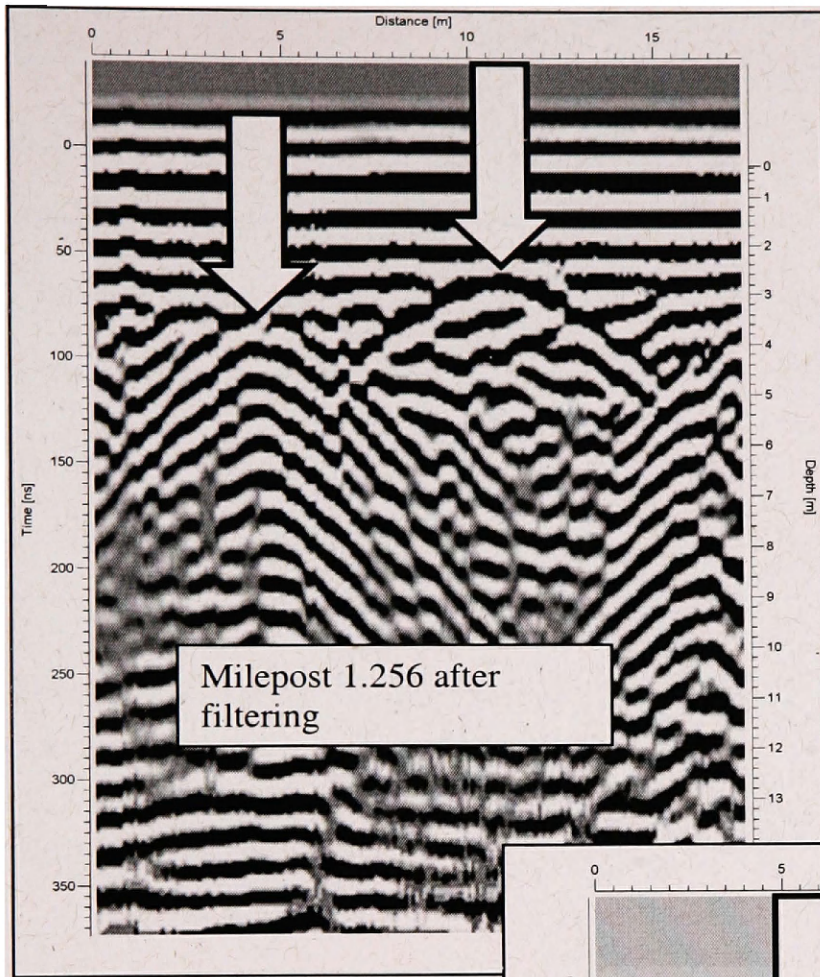
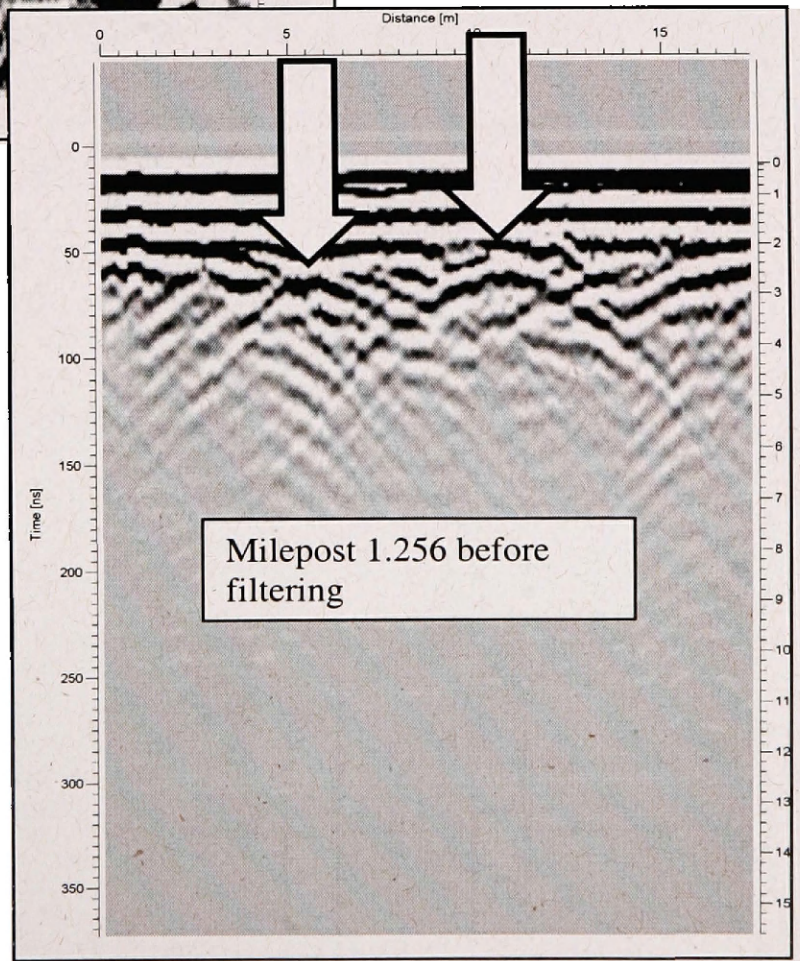


Figure 18. Arrows indicate hyperbolae caused by culverts buried at the Milepost 1.256 location. Ground surface is at 0m depth (right scale). Filters used: DC Offset Removal (107), Band Pass (Upper: 140, Lower: 35), Time Varying Gain (Start: 107, Linear: 100, Exponential: 1).



about one meter, and can't be seen, whereas the culverts in Figure 18 at Milepost 1.256 are readily visible. There is no clear observable bedrock reflection in the GPR images. Scattering due to rocks in the subsurface approaching the signal wavelength (0.85m) is witnessed in many of the culvert images (Figure 20), and the culvert reflections are so strong (when it is at sufficient depth) they take up a majority of the image itself.

Seismic refraction data

Seismic data used to create the profiles beneath the culverts show refractions in the first five meters of this representative seismic profile located at Milepost 4.962 (Figure 21). Excavation occurred at a few of the culvert sites allowing observation of bedrock depth, found to be about two meters at milepost 4.962, consistent with the refractor depth in Figure 21. Velocities of 1070m/s and 2639m/s calculated with SIP[®] software are reasonable for the low-grade metamorphic shale found at Milepost 1.256 and 1.503 (Reynolds, 1997).

Because the geophone spreads extended beyond the culvert more than ten meters in each direction (Appendix B-2), there were data collected on either side away from culvert influence. This led to more reasonable determination of bedrock depth than was possible in the GPR images because the data from those surveys were dominated by the presence of the culverts in many cases. Had data been collected farther from the culvert at each site, a bedrock reflector may have been present and its depth determined. The bedrock depth beneath the culvert could then be interpolated from those calculated depths.

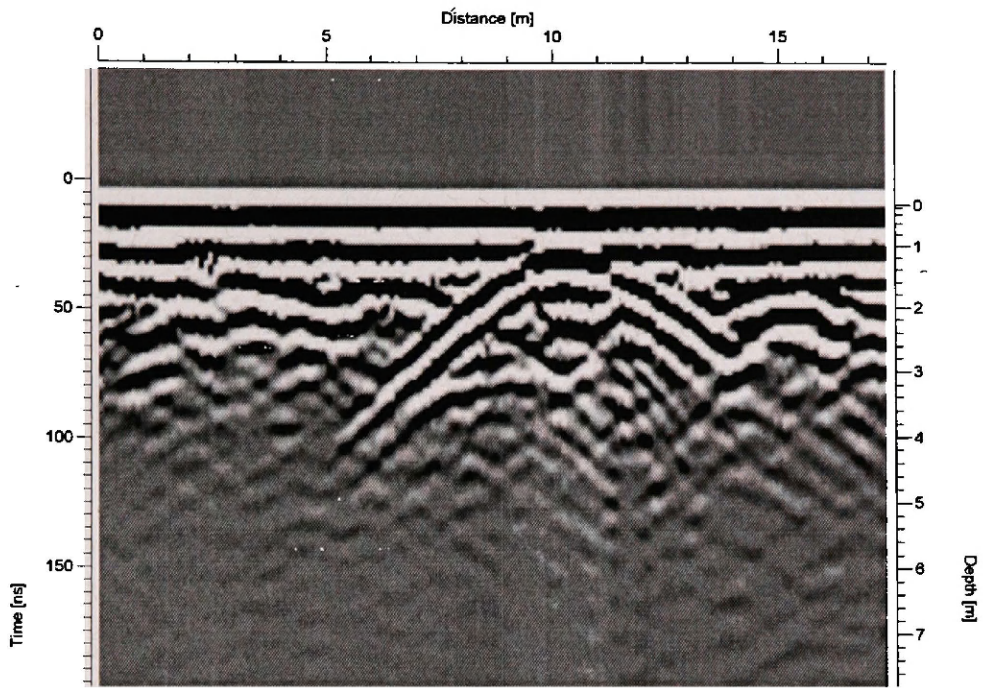


Figure 19. Representative profile showing scattering that can be seen in the first four meters of depth.

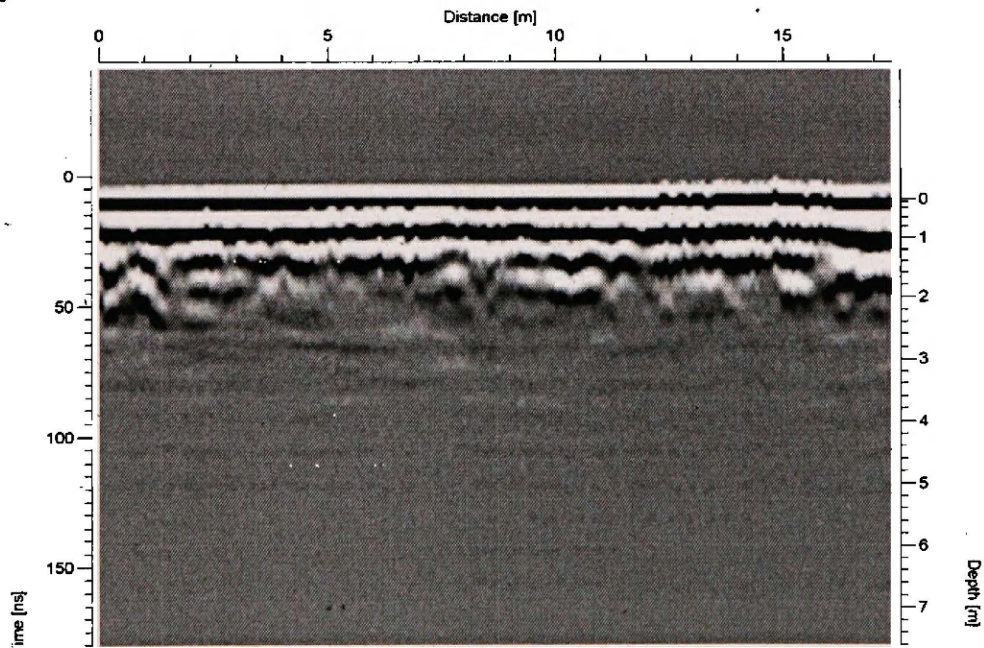


Figure 20. The location of the culvert at this location is at 11.5 meters (top scale). This is the Milepost 4.962 location.

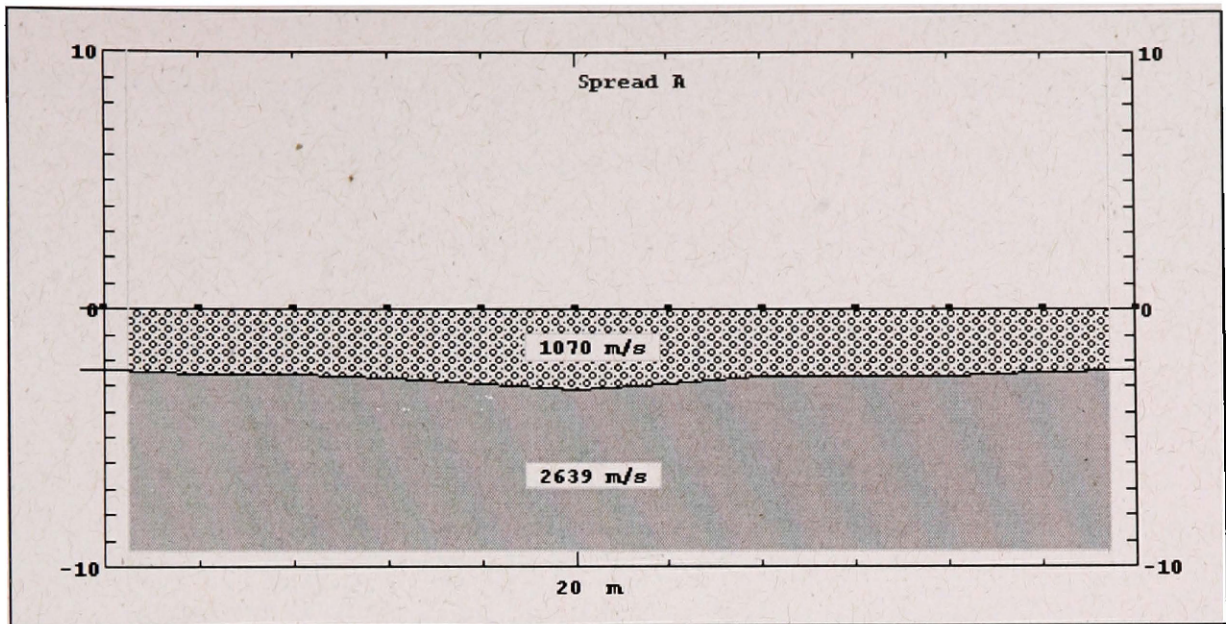


Figure 21. Seismic profile at Milepost 4.962. Excavation at this site confirmed a bedrock depth of about 2 meters.

Benefits and Limitations of GPR at Culvert Sites

GPR is a non-invasive, inexpensive technique that can successfully image the subsurface to the desired depth and resolution. The application of GPR to culvert site analysis is a reasonable method by which to estimate depth to bedrock and thereby approximate the expenditure required to install a culvert at any particular location. Knowing the rippability of an excavation site aids in their prioritization and can minimize cost associated with multiple field visits. GPR surveys can accumulate large amounts of information in short periods of time with few personnel required to successfully perform GPR surveys and maintain quality control of the collected data.

The main problem encountered in surveying at the culvert locations was the culvert itself, acting as such a prominent reflector in the radar images. No information could be obtained about any planar reflectors (bedrock) in the vicinity of a culvert. A solution to this problem would be to tow a GPR antenna at a constant velocity while surveying the entire length of the road. This would provide continuous results over a long enough profile to witness any planar reflectors and interpolate their depth beneath cultural artifacts (culverts). A shielded GPR antenna unit is designed for this application, as it is housed in a protective covered box and often equipped with a wheel allowing surveys to cover a lot of ground. It is important to remember that compact units are only available in the higher antenna frequencies because of the short antenna separation (\leq one meter) required by those higher frequency antennas (100MHz to 1000MHz) with shallower penetration depth (but with higher resolution). Low Frequency (25MHz to 100MHz) unshielded antennas, like the ones used in these surveys, have exposed cables, require antenna separation of one to four meters, and are more appropriate for manual surveying. Researchers at the University of Montana have had success in rigging a towing-sled for lower frequency antennas by attaching the GPR apparatus to a large sheet of vinyl (Hawkins, 2003).

An assessment of velocity made with known reflectors is the most accurate method. However, reasonable estimates are empirically available with CMP surveying techniques. Attention should be directed at the means by which the velocity of the radiowave is assigned when reviewing future GPR survey results. It

should be noted, that due to the manual nature of CMP surveys, it increases the labor-hours and coincidentally the cost associated with the project.

The large amount of data collected during a GPR survey is easily managed. The profiles (such as those created with software packages like Groundvision[®]) are single files unto themselves, and there is no manipulation of the data with the exception of filtering. This is important when considering the cost associated with GPR surveys due to the minimal amount of time spent by Forest employees in handling the data and putting it into presentable form. The filtering process operates from a graphical user interface that allows them to be "turned on or off," enhancing the image at the users' discretion.

Large amounts of data can be collected in relatively small amounts of time. This efficiency in data collection keeps cost low whether equipment is rented or a contractor accomplishes the surveying.

GPR is a non-invasive method for data collection in pristine wilderness areas that are subject to regulation that disallows excavation or construction. This, combined with the reasons above, show GPR to be a cost-effective, non-invasive method by which to collect data.

References

Ayers, J.F., 1990, Shallow seismic refraction used to map the hydrostratigraphy of Nukuoro Atoll, Micronesia: *Journal of Hydrology*, vol. 113, p. 123-133.

Barclay, D.J., Calkin, P.E., Wiles, G.C., 2001, Holocene history of Hubbard Glacier in Yakutat Bay and Russell Fiord, southern Alaska: *GSA Bulletin*, v. 113, p. 388-402.

Belfer, I., Bruner, I., Keydar, S., Kravtsov, A., Landa E., 1998, Detection of shallow objects using refracted and diffracted seismic waves: *Journal Of Applied Geophysics*, vol. 38, p. 155-168.

Beres Jr., M., Heini, F.P., 1991, Application of ground penetrating radar methods in hydrogeologic studies: *Ground Water*, v. 29, p. 375-386

Birkhead, A.L., Heritage, G.L., White, H., van Niekerk, A.W., 1996, Ground Penetrating radar as a tool for mapping the phreatic surface, bedrock profile, and alluvial stratigraphy in the Sabie River, Kruger National Park: *Journal of Soil and Water Conservation*, v.51, p. 234-241.

Burke, K. S., Seismic techniques in exploration of quaternary deposits: *Geoexploration*, vol. 11, p. 207-231.

Carreon-Freyre, D., Cerca, M., Hernández-Marín, M., 2003, Correlation of near-surface stratigraphy and physical properties of clayey sediments from Chalco Basin, Mexico, using Ground Penetrating Radar: *Journal of Applied Geophysics*, vol. 53, p. 121-136.

Gerlitz, K., Knoll, M.D., Cross, G. M., Luzitano, R. D. and Knight, R., 1993, Processing Ground Penetrating Radar Data to Improve Resolution of Near-Surface Targets, in *Proceedings, Proc. of the Symposium on the Application of Geophysics to Engineering and Environmental Problems*, San Diego, Vol. 2, pp. 561-574.

Haeni, F.P., McKeegan, D.K., Capron, D.R., Ground penetrating radar study of the thickness and extent of sediments beneath Silver Lake, Berlin, and Meriden, Connecticut: *U.S. Geological Survey Water-Resources Investigations Report 85-4108*, 19 p.

Harvey, N., 1977, Application of shallow seismic refraction techniques to coastal geomorphology: A coral reef example: *CATENA*, vol. 4, p. 333-339.

Hawkins, C.R., 2003, Imaging the Shallow Subsurface using Ground Penetrating Radar at the Nyack Floodplain, Montana [M.S. Thesis] Missoula: University of Montana, 35p.

Holmes, W.F., Dorava, J.M., 1995, Overview of Environmental and Hydrogeologic Conditions at Yakutat, Alaska: U.S. Geological Survey Open-File Report 94-713, 17 p.

Huggenberger, P., Meier E., Pugin, A., 1994, Ground-probing radar as a tool for heterogeneity estimation in gravel deposits: advances in data-processing and facies analysis: *Journal of Applied Geophysics*, v. 31, p. 171-184.

King, G.S., 1995, Surficial Geology and Preliminary Chronology of Russell Fiord, Alaska [MA Thesis]: Buffalo, University of New York, 103 p.

Nakashima, Y., Zhou, H., Sato, M., 2001, Estimation of groundwater level by GPR in an area with multiple ambiguous reflections: *Journal of Applied Geophysics*, p. 241-249.

Olheoft, G.R., 2000, Maximizing the information return from ground penetrating radar: *Journal of Applied Geophysics*, vol. 43, 175-187.

Oneal, M.L., McGeary, S., 2002, Late Quaternary stratigraphy and sea-level history of the northern Delaware Bay margin, southern New Jersey, USA: a ground penetrating radar analysis of composite Quaternary coastal terraces: *Quaternary Science Reviews*, vol. 21, p. 929-946.

van Overmeeren, R.A., 1994, Georadar for hydrogeology: *First Break*, v. 12, p. 401-408

Pant, P.R., Murty, B.S.R., 1981, Rapid seismic refraction delay-time profiling technique for shallow bedrock studies: *Geoexploration*, vol. 18, p. 269-280

Reynolds, J.M., 1997, *An Introduction to Applied and Environmental Geophysics*: New York, John Wiley and Sons, 796 p.

Russell, J.K., Cagnoli, B., 2000, Imaging the subsurface stratigraphy in the Ubehebe hydrovolcanic field (Death Valley, California) using ground penetrating radar: *Journal of Volcanology and Geothermal Research*, vol. 96, p. 45-56

Sain, K., Reddy, P.R., Behera, L., 2002, Imaging of low-velocity Gondwana sediments in the Mahanadi delta of India using travelttime inversion of first arrival seismic data: *Journal of Applied Geophysics*, vol. 49, p. 163-171.

Sandberg, S.K., Slater, L.D., Versteeg, R., 2002, An integrated geophysical investigation of the hydrogeology of an anisotropic unconfined aquifer: *Journal of Hydrology*, v. 267, p. 227-243.